Copyright © 1982 American Telephone and Telegraph Company
THE BELL SYSTEM TECHNICAL JOURNAL
Vol. 61, No. 6, July–August 1982
Printed in U.S.A.

Simulation and Design Studies of Digital Subscriber Lines

By S. V. AHAMED

(Manuscript received July 14, 1981)

To investigate the feasibility of transmitting data bidirectionally between 56 and 144 kb/s, an extensive simulation and experimental study was undertaken. The computational techniques for the study have been developed and coupled to a large data base, which contains the individual loop configurations of a statistically significant population of the Bell System loop plant. Two modes of transmission (the hybrid and the time-compression multiplexing) are investigated thoroughly by computational techniques, and the simulated plots are compared with experimentally generated oscillograms. These results are displayed graphically by eye diagrams for individual loops and by scatter plots for all the loops in the data base. Different varieties of scatter plots display different attributes of eye diagram. Broad spectrums of such results are cross-compared to choose optimal systems and circuit configurations for a particular mode of transmission at a particular bit rate. Effects of varying terminating networks are also studied and the extent of echo cancellation necessary is investigated by studying the amplitude and the shape of near-end reflections. Various codes are investigated even though the primary emphasis has been on the bipolar code. Major conclusions are summarized in the concluding remarks.

I. INTRODUCTION

Digital data transmission over existing loop plant facilities has been envisioned by numerous organizations around the world. In Japan,[1,2] initial designs for digital data transmission rates up to 64 kb/s are being investigated. In Switzerland, there has been initial interest[3] to provide an overall transmission rate of up to 160 kb/s. In Sweden, an 80-kb/s burst system, operating at 256 kb/s in 125-μs slots has been investigated.[4] In Norway,[5] digital pulse-code modulation (PCM) hybrid

transmission rates greater than 64 kb/s (up to 80 kb/s) have been analyzed. In Great Britain, hybrid 64-kb/s channels have been proposed[6,7] by superimposing them over the baseband analog telephone communications. Other Western European countries[8,9] (Germany, France, and Italy) have started discussion of high-speed digital transmission.

In the Bell System, the results of preliminary investigations have been reported.[10,11,12] This paper presents the computer simulations and the entire cross section of results obtained from the extensive simulations that have been performed using a loop plant data base in conjunction with specific terminal systems. The simulations test the functioning of any given system with existing loops from the 1973 Loop Survey,[13] they test the effects of component design variations, and variations of such factors as temperature, loop configuration, etc., and, finally, they verify the eye opening performance at different bit rates.

The paper also presents the results of such simulations under two major modes of transmission: (*i*) a full-duplex simultaneous bidirectional transmission of data with a hybrid and active echo canceler (hereafter referred to as the hybrid system), and (*ii*) the time-compression multiplex ["burst" or the "ping-pong" system (hereafter referred to as the TCM system)].

The remainder of the paper covers five major sections. Each section addresses a specific issue in the overall design. Section II gives the simulation techniques and data base organization. (The Appendixes contain the mathematical framework of the computation.) In Section III, the electrical characteristics of the loop plant, as they pertain to the transmission of data (2.4 to 324 kb/s), are tabulated. Some of the physical data are also given to indicate the wide variety of loops in the plant. Section IV described the time-domain simulations (with numerous codes) which yield wave shapes and eye diagrams at the receiver. Section V compares the performances of different systems at different rates between 56 to 324 kb/s. Results are summarized as scatter plots, each showing an attribute of the eye diagrams for all the loops in the data base. Section VI describes a computer-aided design technique for evolving an optimal equalization strategy. The effects of different equalizer designs on the eye openings at the receiver is also documented. Finally, the concluding remarks give the overall summary of findings.

II. TECHNIQUES: SIMULATION, DATA BASE, AND ORGANIZATION STRATEGY

2.1 Introduction

Any repetitive periodic phenomenon may be analyzed by Fourier analysis. To study the transmission system response, we resort to a

long periodic sequence (48 pulses) of randomly distributed data. The flexibility of analyzing the system performance in the spectral domain becomes available before inverting the Fourier series to obtain the time-domain response. The process is carried out independently for the two directions of data transmission over one pair of wires. Simultaneous bidirectional transmission performance evaluation in the hybrid system entails calculation of reflections arising because of cable and termination mismatch at all the harmonics of the overall repetitive period. The transmission rate is the line rate. The TCM transmission, however, is unaffected by near-end reflections since data transmission is multiplexed in the time domain by increasing the transmission rate to 2.25 times the information rate.

To evaluate the system performance on individual loops, it is necessary to access data bases which store statistical samples of loop compositions of the existing loop plant. Thus, the simulation capability performs four functions: computations, data base manipulations, generation of graphical displays, and provision of a capability for evaluation and optimization of the system components. The first three of these functions need minimal operator intervention, and the last function is interactive with the system designer.

2.2 The Basic concepts in time-domain simulations

Transmission of digital data is a time-domain phenomenon. However, electronic circuitry and cable characteristics are better defined in the spectral domain. Hence, to simulate the entire physical process of the data transmission, we resort to a limit-cycle[14] approach. The entire system—the electronic circuitry and the individual loop under study is forced into a periodic function in which the boundary conditions at the beginning and the end of a predefined period are identical. The approach facilitates the transformation of the cyclic time-domain phenomenon into its harmonic spectral-domain components by Fourier series. Enough flexibility is provided to alter the mode of excitation to correspond to any random or specified pulse pattern within a sufficiently long period.

2.3 Spectral-domain considerations

Spectral-domain responses are essential subsets that can be isolated from time-domain simulations. To provide systematic computations, the spectral-domain and time-domain simulations access identical data bases and subprograms. The data base generation and display programs are separate. They have been completely automated to generate and graphically display predefined component and system characteristics.

2.4 Representational techniques

2.4.1 Excitation signals

A 48-pulse period* spans the repetitive cyclic time. Any random or prespecified pattern of pulses are transmitted in either direction. Delta function or finite-width pulses have been simulated with different coding (alternate bipolar, ternary, polar, etc.) options.

Sixty-four Fourier harmonics represent the pulses. This choice reflects the presence of filters with a sharp roll-off beyond the system cutoff frequency. The truncation at 1-1/3 bit rate (i.e., 64/48) has little effect on the accuracy of the simulation, but cuts the core requirement and execution time.

2.4.2 Component representation

Bidirectional data transmission systems generally have a transmitter, a loop, a filter, an equalizer, a terminating impedance, and a device to limit the near-end reflections.† For the delta functions or finite pulse-width multilevel pulses at the transmitter, the excitation functions are defined in Appendix A. The loop (Section 2.4.3) is characterized by ABCD matrices (one set for each harmonic frequency). The filter is represented by standard transfer functions. The equalizer is programmed by the distribution of poles and zeros. The matching impedance being passive has a simpler characterization. Finally, the isolating device which separates the received and transmitted signal is represented in the frequency domain (for frequency-domain cancellation circuits) or in the time domain (for CCD-type transversal filter circuits). The technique of the computation of the cancellation signal varies appropriately. In the TCM mode of transmission, the contaminating signal is ignored because the transmitter is inactive during the reception of the signal and vice versa.

2.4.3 Loop representation

The loop constitutes the most variable component in the entire system. A summary of Bell System loop statistics has been reassembled in a dedicated data base. Composite loops (with numerous loop sections and bridged taps) are represented by their individual ABCD matrices at each harmonic frequency. The temperature of cable (aerial vs. buried) sections can vary drastically. Hence, temperature distributions are also permitted in the simulation by an identifier scheme to indicate particular lengths which experience the differential temperatures.

---

* The 48-pulse period is an arbitrary duration. The limited core capacity of the dedicated computer was the primary reason for the choice. More recently, we have been able to extend the simulations to 480 pulses and 1200 harmonics.

† Typical examples are echo cancelers, hybrids, frequency-domain cancellation circuits, or time-division switches.

The R, L, G, and C parameters, at different temperatures for different lengths, are calculated by accessing a separate data base, storing the primary parameters[15] and their temperature variations.

2.5 Computational techniques

2.5.1 System components

Conventional circuit analysis of components is performed by accepting critical resistors, capacitors, and transistor data. Noncritical components are represented by transfer functions. When the sensitivity analysis is performed, individual components are perturbed. When the sensitivity of system blocks is analyzed, the transfer functions are perturbed. Cascading appropriate ABCD matrices for the loop sections leads to composite loop ABCD parameters (see Appendix B). These parameters are generated from the central office to the subscriber, and the A and D terms are interchanged for the other direction, thus reducing the core requirements and execution time. The terminating impedance effects are computed by multiplying the ABCD matrix of the cable (with adequate attention to the direction of transmission) by the ABCD matrix of the terminating impedance.

2.5.2 Restoration to time domain

The excitation function has obvious poles at $p = 2\pi im/T$ ($m = 1, 2, \cdots, M$) and the computational technique for evaluating the normal Fourier integral becomes converted to the summation of (M) harmonics responses over K pulse periods (see Appendix C). The two highlights before the double summation in eq. (10) (see Appendix C) are (i) the entire transfer function of the total system including filters, equalizers, and any echo cancelers [i.e., $\zeta(p)$, see eq. (6), Appendix C] can be obtained after finding the composite ABCD parameters for both directions of transmission, and (ii) the use of L'Hôpital's rule in evaluating the residues at the M poles [see eq. (9), Appendix C].

2.5.3 Simulation of echo cancellation

During simultaneous bidirectional transmission of data, the near-end echo adds to the received signal within the hybrid. There are two ways of simulating the echo-canceler function. The first one consists of computing the total signal (reflections and the received pulses), and then subtracting the reflection out systematically. The second method consists of systematically dropping all, or a large fraction, of the frequency-domain reflected signal before summing the Fourier components.

2.5.4 Echo cancellation signal from single-pulse response

The reflections of a single-pulse excitation from the Central Office

(co) side and then from the subscriber (s) side are stored. There are 240 time positions covering the 48-pulse period. These responses are then shifted by the same amount that any new pulse is shifted from the original pulse that gave the first reflection. The response of the pulses occupying the 48 time slots of random excitation is obtained as a summation of all the responses suitably displaced from the location of the original pulse. Since the excitation is assumed to be periodic, any overflow beyond the 240 time positions is reaccumulated at the beginning of the period.

The subtraction of the reflected signal from the total signal by the echo canceler is carried out by either of two ways: (*i*) prespecified fraction (between 90 to 99 percent) of the total reflected signal is systematically subtracted from the total signal at the received end, and (*ii*) a randomly varying fraction averaging to a prespecified number (90 to 99 percent) of the total reflected signal is subtracted from the total received signal. The reason for the use of a second procedure was to reflect the uncertainties caused by the convergence in the tap weight setting of a real echo-canceler device. These settings can change slightly because of the number of iterations the device has experienced at any instant of time. Being an adaptive device, the setting varies by small increments around the average value with time, and the second computational procedure reflects this uncertainty. For the illustrations presented here, the first procedure of echo cancellation is used since the second one causes a small random perturbation of the data* obtained in the first.

2.5.4.1 ***Simplified echo cancellation.*** The simulation of the echo canceler is done by suppressing the addition of the reflected signal in the frequency domain before summing the Fourier components. The inaccuracy of this technique is because the time events are only approximated by the Fourier expansion in view of the truncation of the harmonics. These inaccuracies are not consistent in the representation of the limit cycle encompassing a finite number of pulses (48 in this case) with the inaccuracies in the representation of a single pulse whose reflection was determined in the former case. In the latter case, only a percentage (90 to 99 percent, depending on the quality of the echo canceler) of each of the harmonics of the entire 48-pulse period is subtracted. In the former case, the specified percentage of the total reflected signal in the time domain was subtracted out. However, the simplicity of the simulation procedure has prompted the use of the latter method in most cases after determining that the difference of the echo suppressions by the two methods does not cause more than

* Very marginal eyes are occasionally closed, and an occasional error of the marginal bit occurs.

a 2- to 3-percent change in the eye openings in either the CO side or the S side.

2.6 Establishment of permanent bases

The primary data bases consist of three permanent files: (*i*) the cable characterization, (*ii*) the Loop Survey files holding the loop composition of all the 1973 survey loops up to the 18-kft loop without bridged taps, and (*iii*) the files containing the same loops including details of bridged-tap locations and composition.

2.6.1 Access and reuse of selected bases

Very long computations yield large files, and unless some systematic steps are taken to conserve the disc space, results obtained from different systems of different components cannot be easily cross-compared. Hence, certain disc files or a group of files are reused continuously. A typical group of such files holds excitation pulse patterns and their harmonics, filter transfer functions, equalizer transfer function (if it is amenable to such a representaion), single-pulse response function (if it is to be used in conjunction with an echo canceler), etc. It is also necessary for the intermediate computations to be completed before the reuse of the allocated disc space. A typical example of such a situation is after the generation of the time-domain received pulse data from the spectral domain. The eye statistics (eye openings, top, central, bottom-eye thicknesses, and the eye height) have to be computed from a separate program before the files holding the time-domain response can be reused. Hence, the use or reuse of intermediate data bases needs special consideration in the overall architecture of the system.

2.7 Conclusions

In Section II, the major highlights of the software simulation system are presented. Numerical algorithms, computations, and functions are organized independently of the major housekeeping and file management functions. The entire system has been tailored to work efficiently and smoothly on dedicated minicomputers. System capabilities range from simply analyzing the data for statistical characteristics from the data bases to the entire system simulation under data transmission and the analysis of failure rates, details of eye closure, and sensitivity analysis of components.

III. FUNDAMENTAL LOOP PLANT STATISTICS FOR DIGITAL DATA TRANSMISSION

3.1 Introduction

Possible data transmission rates envisioned for the future range

from 56 to 324 kb/s. A set of seven bit rates (2.4, 4.8, 9.6, 64, 144, 216, and 324 kb/s) is chosen to span the range of interest. The 1973 Loop Survey presents a cross section of loops that may be expected to carry the data traffic. However, they may be generally limited to a loop length of 18 kft because of the presence of loading coils beyond this distance. This section presents characterization of the loops in two loop configurations: (*i*) with all bridged taps stripped, and (*ii*) with all bridged taps intact. Image impedances (at the half-bit-rate frequencies 1.2, 2.4, 4.8, 32, 72, 108, and 162 kHz) are also presented. The physical statistical data are presented in condensed form and selected electrical parameters are also tabulated.

3.2 Organization of results (loops with bridged taps stripped)

3.2.1 Physical characteristics

Eliminating loops longer than 18 kft, those with loading coils, and nonstandard cable sections, about 76 percent (831* loops) of the 1098*-loop population surveyed[13] constitutes the truncated data base over which the digital data transmission studies are based. A histogram relating the population to distribution of the loops by their length and the number of cable section(s) is shown in Fig. 1a. The typical overall composition of an average loop (in the truncated population), which is 7748.63 ft long, has 4500.59 ft of No. 26 AWG cable with 2408.47 ft of No. 24 AWG cable, 797.52 ft of No. 22 AWG cable and, finally, with 42.03 ft of No. 19 AWG cable. Figure 1b shows the average composition of the loops in each kft band between 0 to 18 kft.

3.3 Typical results generated at 32 kHz for 64-kb/s rate (loops with bridged taps stripped)

There are three sets of results for the three temperatures (140°F, 60°F, and 0°F) at which the simulation is done over all the loops in the data base. This section gives the typical results at 60°F. In Figs. 2 and 3, the loop attenuations are shown as scatter plots of the individual attenuation of each loop. Figure 3 gives the data when the attenuation is plotted against the converted loop length. The conversion of the actual loop length to its equivalent No. 22 AWG cable length is done by first determining the equivalency numbers between cable length for a given attenuation and then by cumulating the length of each loop section in terms of its equivalent length.

In Figs. 4 and 5 the resistive component of the impedance is plotted against the reactive component for each of the loops at 32 kHz and 60°F. Denser clusters of points are detected around the impedance

* For clarification, "loop survey" refers to the 831-loop data base, and "Loop Survey" refers to the original 1098-loop data base.

(147–j94) ohms of No. 26 AWG cable. This result reinforces the dominance of No. 26 AWG cable also represented in Fig. 1a.

3.4 Summary of results (loops with bridged taps stripped)

At each frequency and at each temperature, the high, low, and average values of the most important parameters are tabulated (see Table I). In addition, two specific parameters evolve from this computation: (*i*) the gauge conversion factor for equalization, and (*ii*) the temperature length equivalency number. The first parameter becomes critically important while determining the equalization required to compensate for mixed gauge loops at any particular frequency. For the digital transmission, we have found that if the conversion numbers estimated at half-baud-rate frequency are used consistently at all harmonic frequencies of the pulse pattern, the eye diagrams predicted after the analysis very closely match those obtained by an experimental procedure. Hence, for data transmission at 216 kb/s, 1 kft of Nos. 19, 24, and 26 AWG cables yield the same loss as 0.648, 1.408, and 1.923 kft of the No. 22 AWG cable. These results are obtained by plotting the loss of the various gauges at 108 kHz, and then proportioning the lengths.

The second conversion number is also obtained by a similar procedure. The equivalent change in the length, caused by every degree change in temperature, is evaluated by plotting the losses at numerous temperatures, and then a coefficient of temperature sensitivity is obtained by proportioning the length accordingly.

This coefficient α, which relates the length (l_2 in feet) at temperature t_2°F and the length (l_1 in feet) at temperature t_1°F, is defined as

$$l = l_1[l + \alpha(t_2 - t_1)] \text{ ft.}$$

Coefficient α has been evaluated as 2.135×10^{-3} per degree F, at 108 kHz. This number becomes important in determining the equivalent length of loops in terms of No. 22 AWG cable at 55°F.

3.5 Organization of results (loops with bridged taps intact)

3.5.1 Physical characteristics

The truncated data base consisting of 831 loops has a total of 1365 bridged taps. The average loop is 7748.63 ft long, has approximately four sections, and has 1.64 bridged taps on it. The length of an average tap is 922.42 ft, consisting of about 54 percent of No. 26 AWG, 33 percent of No. 24 AWG, 12 percent of No. 22 AWG, and less than 1 percent of No. 19 AWG cable composition. The median distance between the CO and the first tap is 6523 ft, and the median distance between the first and second taps is 1071 ft. Loops between 0 to 1 kft have the longest average length of bridged tap—1333.3 ft, with 1.15

Table I—Maximum, minimum, and average values of loop impedances at different frequencies (no bridged taps)

		Central Office Side of Loops (Zin)						Subscriber Side of Loops (Zin)					
	Degrees	Maximum		Minimum*		Average		Maximum		Minimum*		Average	
kb/kHz	F	Re	Im	Re	Im	Re	Im	Re	Im	Re	Im	Re	Im
2.4/1.2	140	744	−696	400	−400	649.3	−628.8	720	−544	416	−380	632.0	−634.1
	60	680	−644	376	−376	607.6	−586.9	664	−660	388	−352	593.9	−592.3
	0	632	−616	368	−332	572.7	−552.0	640	−616	352	−344	561.7	−557.0
4.8/2.4	140	544	−500	272	−270	466.4	−443.1	512	−500	264	−265	446.6	−443.8
	60	504	−456	256	−256	437.1	−412.5	480	−456	264	−240	420.4	−414.4
	0	480	−432	240	−240	412.5	−387.0	456	−344	256	−228	398.2	−389.6
9.6/4.8	140	400	−365	190	−180	336.6	−311.2	380	−350	180	−190	318.5	−307.1
	60	370	−325	190	−160	316.7	−288.7	360	−325	165	−160	300.4	−286.1
	0	360	−300	180	−155	299.9	−269.8	340	−290	162	−155	285.2	−268.4
64/32	140	170	−110	97	−22	144.6	−93.1	170	−110	85	−16	138.3	−86.8
	60	170	−101	92	−16	140.4	−83.9	165	−100	85	−14	134.4	−78.2
	0	168	−94	92	−14	136.9	−76.3	160	−96	85	−12	131.3	−70.9
144/72	140	145	−67	90	−17	120.4	−51.3	150	−70	90	−8	117.4	−47.2
	60	145	−60	90	−15	119.4	−45.3	147	−61	86	−7	116.6	−41.7
	0	145	−55	90	−11	118.7	−40.5	145	−37	83	−6	116.1	−37.1
216/108	140	134	−54	85	−6	114.1	−37.4	140	−50	89	−6	112.0	−34.7
	60	134	−50	86	−5	114.0	−32.9	140	−46	90	−4	112.1	−30.5
	0	134	−45	86	−4	114.1	−29.3	136	−43	94	−1	112.2	−27.1
324/162	140	130	−40	86	−6	110.1	−27.4	134	−42	87	−5	108.1	−25.7
	60	132	−34	88	−3	110.6	−24.1	132	−40	86	−3	108.8	−22.7
	0	134	−36	90	−1	111.1	−21.5	134	−39	88	−1	109.3	−20.3

* The low numbers in these columns are not very accurate, since they are not program generated; instead, they are all scaled from the scatter plots.

bridged taps for each loop. The average composition of each bridged tap is 59.3, 37.0, 3.7, and 0.0 percent of Nos. 26, 24, 22, and 19 AWG cables. The total number of loops in this kft band is 20, and 17 of these do have bridged taps. The average loop length is 776 ft.

Loops between 17 to 18 kft have the highest average number (2.87) of bridged taps per loop. The average loop length is 17,331.19 ft, and the average bridged tap is only 626.9 ft. The average composition of the bridged tap is 10, 74.0, 16.0, and 0.0 percent of Nos. 26, 24, 22, and

Table II—Bridged-tap distribution by loop lengths (0 to 18 kft)

Loop Length in Feet	No. of Bridged Taps	No. of Loops, No Bridged Taps	No. of Loops
0–1000	23	3	20
1000–2000	48	6	38
2000–3000	82	4	56
3000–4000	104	13	69
4000–5000	104	12	64
5000–6000	115	16	77
6000–7000	114	5	64
7000–8000	115	7	72
8000–9000	121	5	67
9000–10,000	97	3	53
10,000–11,000	96	8	55
11,000–12,000	87	8	52
12,000–13,000	59	3	38
13,000–14,000	50	5	31
14,000–15,000	45	1	26
15,000–16,000	32	3	21
16,000–17,000	27	0	12
17,000–18,000	46	2	16
Total no. of loops = 831	Loops: No bridged taps = 104		Loops with bridged taps = 727

Table III—Average loop length and average bridged-tap length distribution

Loop Length in Feet	Average Loop Length	Average No. of Bridged Taps	Average Bridged-Tap Length
0–1000	776.00	1.15	1333.35
1000–2000	1559.74	1.26	995.58
2000–3000	2548.87	1.46	782.12
3000–4000	3544.38	1.51	1121.13
4000–5000	4539.55	1.62	939.42
5000–6000	5445.13	1.49	962.14
6000–7000	6481.23	1.78	740.68
7000–8000	7483.33	1.60	957.54
8000–9000	8541.78	1.81	904.93
9000–10,000	9446.68	1.83	848.39
10,000–11,000	10572.91	1.75	843.49
11,000–12,000	11466.83	1.67	1092.56
12,000–13,000	12435.87	1.55	938.66
13,000–14,000	13383.77	1.61	932.66
14,000–15,000	14412.73	1.73	917.27
15,000–16,000	15447.76	1.52	926.06
16,000–17,000	16490.17	2.25	1016.19
17,000–18,000	17331.19	2.87	626.91
Total no. of bridged taps = 1365	Average length of bridged taps = 922.42		

Table IV—Maximum, minimum, and average values of loop impedances at different frequencies (with bridged taps)

		Central Office Side of Loops (Zin)						Subscriber Side of Loops (Zin)					
	Temperature	Maximum		Minimum		Average		Maximum		Minimum		Average	
kb/kHz	°F	Re	Im	Re	Im	Re	Im	Re	Im	Re	Im	Re	Im
2.4/1.2	140	704.8	−639.7	176.8	−513.2	560.0	−499.2	649.9	−640.	178.3	−120.6	497.47	−533.24
	60	652.3	−597.5	160.4	−478.3	520.8	−467.7	609.6	−597.5	161.5	−114.7	471.19	−497.8
	0	606.8	−562.1	147.8	−449.7	488.8	−440.9	575.8	−562.1	148.6	−109.5	448.5	−468.0
4.8/2.4	140	520.4	−453.0	123.4	−364.3	411.8	−343.1	476.3	−449.9	131.8	−78.8	340.5	−340.47
	60	486.0	−418.9	120.3	−337.3	383.6	−321.7	440.7	−419.5	123.9	−73.5	323.9	−346.9
	0	456.8	−393.5	117.3	−315.3	360.2	−303.4	412.1	−394.4	117.3	−69.5	309.6	−326.6
9.6/4.8	140	393.1	−324.8	91.5	−259.8	303.3	−230.7	351.6	−314.1	80.4	−57.2	234.5	−252.5
	60	371.5	−302.1	83.3	−239.0	284.2	−215.8	331.0	−292.6	78.6	−49.2	223.9	−236.5
	0	349.4	−281.4	77.6	−221.83	268.4	−203.2	313.2	−274.3	78.3	−44.5	214.9	−222.8
28/56	140	204.4	−129.7	48.8	−97.2	150.3	−100.7	198.8	−128.9	31.2	−9.5	106.6	−82.4
	60	198.7	−119.5	44.7	−87.3	145.2	−82.4	188.9	−117.6	30.5	−7.0	103.8	−76.0
	0	193.9	−112.4	41.8	−79.1	141.1	−67.1	178.0	−109.2	30.2	−5.4	101.6	−70.6
32/64	140	196.0	−120.1	47.1	−88.9	144.3	−99.1	193.2	−121.0	28.9	−4.3	102.3	−74.7
	60	194.7	−112.2	43.8	−79.6	139.9	−82.0	188.3	−112.2	29.1	−0.9	99.8	−68.7
	0	192.9	−105.5	40.3	−71.9	136.4	−67.0	181.3	−103.2	28.6	+2.6	98.0	−63.7
40/80	140	187.8	−108.9	44.7	−76.1	135.7	−95.2	177.9	−105.0	25.5	+3.1	96.1	−63.2
	60	189.8	−99.4	43.9	−67.7	132.3	−82.2	181.3	−100.5	24.9	+8.9	94.2	−57.8
	0	189.6	−94.8	41.8	−60.8	129.7	−70.2	183.1	−96.6	24.8	+15.3	92.9	−53.4
72/144	140	187.1	−101.7	40.3	−49.3	120.5	−67.5	157.6	−84.3	21.5	+27.8	85.2	−39.7
	60	190.5	−98.4	40.1	−43.2	119.4	−62.4	164.1	−84.5	21.3	+43.7	84.6	−35.9
	0	192.0	−93.0	40.1	−38.3	118.7	−57.6	175.3	−85.7	21.2	+54.6	84.2	−32.8
96/192	140	206.7	−79.7	38.6	−39.5	115.8	−49.6	180.3	−84.1	19.4	+49.7	82.6	−31.5
	60	233	−80.2	38.6	−34.5	115.4	−49.6	186.8	−83.5	20.3	+54.4	82.5	−28.1
	0	253.3	−81.1	38.7	−30.5	115.2	−50.6	200.7	−85.1	18.9	+56.8	82.4	−25.4
108/216	140	212.2	−105.5	37.9	−36.1	114.4	−38.0	180.1	−82.7	16.3	+59.4	81.8	−29.0
	60	198.8	−111.5	38.0	−31.5	114.2	−36.8	194.0	−81.4	16.5	+68.5	82.0	−25.9
	0	201.8	−114.2	38.1	−27.8	114.2	−37.5	203.1	−84.4	16.8	+74.9	82.1	−23.3
162/324	140	216	−119.7	35.1	−26.7	110.2	−34.6	184.8	−100.6	15.2	+74.5	78.5	−22.4
	60	233.4	−133.4	35.4	−23.4	110.7	−27.9	213.6	−105.3	14.0	+81.4	79.2	−20.3

Table V—Maximum and average attenuation of loops

kb/kHz	Temperature (°F)	Attenuation in dB	
		Maximum	Average
2.4/1.2	140	11.7	4.93
	60	10.7	4.49
	0	9.9	4.13
4.8/2.4	140	15.6	6.92
	60	14.1	6.29
	0	13.3	5.78
9.6/4.8	140	21.5	9.63
	60	19.5	8.73
	0	18.0	8.01
28/56	140	45.5	19.93
	60	41.0	17.75
	0	37.4	16.02
32/64	140	47.6	20.82
	60	42.9	18.50
	0	39.1	16.66
40/80	140	50.6	22.27
	60	45.6	19.72
	0	41.7	17.72
72/144	140	60.0	26.30
	60	53.3	23.22
	0	47.9	20.84
96/192	140	66.2	28.46
	60	60.5	25.21
	0	56.4	22.73
108/216	140	69.1	29.44
	60	61.9	26.13
	0	56.4	23.62
162/324	140	76.0	33.15
	60	69.0	29.68
	0	63.5	27.08

19 AWG cables, respectively. Between these extremes (shortest loops with longest bridged taps and longest loops with shortest bridged taps) lies a population whose average bridged tap length is fairly consistent. Even though the population density is sparse, the in-extreme bands of length (0 to 1 kft and 17 to 18 kft), the population density in the intermediate bands (Table II) is relatively high and the statistical information derived is dependable. These statistics are tabulated in Tables II and III. The percentage of loops having bridged taps ($\geq$0, $\geq$1, $\geq$2, etc.) is shown in Fig. 6. Figure 7 (compare against Fig. 1a) displays the gauge distribution in the bridged tap. These distributions indicate similar patterns with a dominance of No. 26 AWG cable, which is gradually replaced by No. 24 AWG cable as the length of the loop

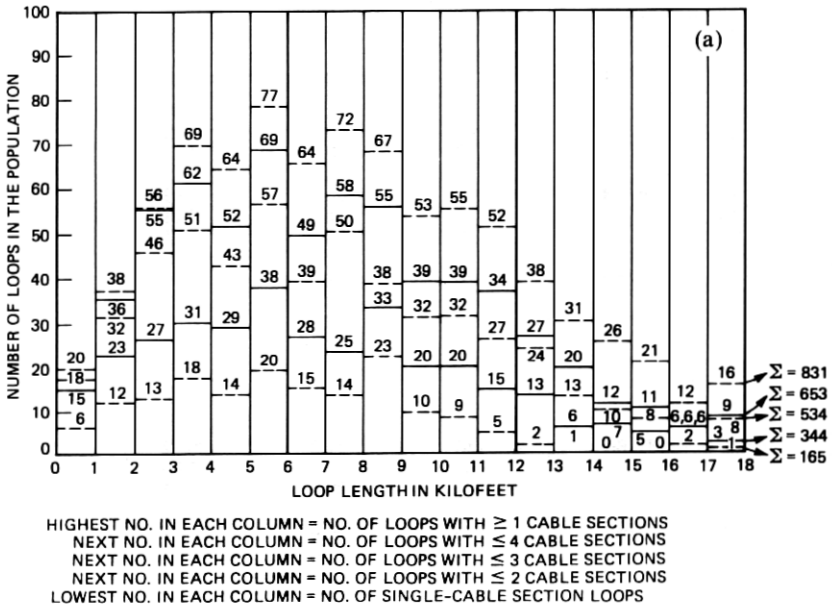

Fig. 1a—Histogram of loop population distribution by number of cable sections in each kft.

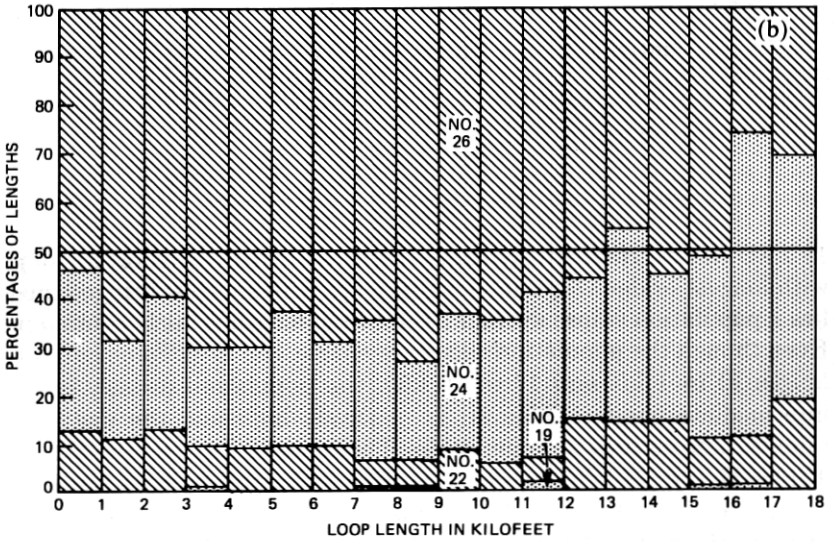

Fig. 1b—Distribution of gauge numbers with loop length.

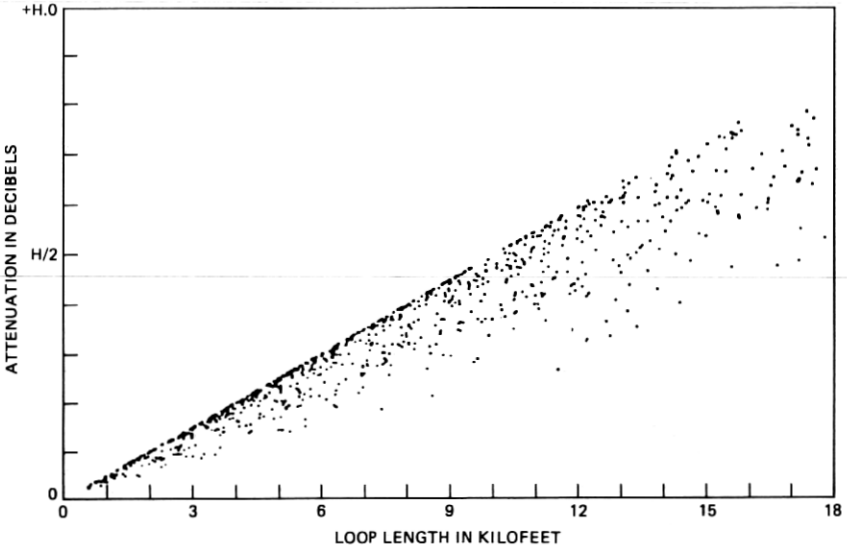

Fig. 2—Scatter plot of loop attenuations plotted against the loop length at 32 kHz and 60°F. The *X*-scale is 1 kft per division and *Y*-scale is 5.0 dB/division.

increases. Numbers 22 and 19 AWG cables do not dominate either the bridge tap or the loop lengths.

3.6 Summary of results (loops with bridged taps intact)

The loops in the survey have been simulated at three temperatures (140°F, 60°F, and 0°F). However, the discrete frequencies have been expanded to include (28, 40, and 96 kHz for 56, 80, and 192 kb/s rates). A summary of the image impedance at the ten discrete frequencies (1.2, 2.4, 4.8, 28, 32, 40, 72, 96, 108, and 162 kHz) is tabulated in Table IV. Table V gives a summary of loop attenuations.

3.7 Conclusions

The loop plant environment is far from the ideal situation where uniform gauge wires run from the CO to the S. Any design of the bidirectional data transmission facility has to accommodate the wide disparity of cable compositions, bridged-tap configurations, and highly variable impedances looking from either direction of the loop. The range and statistics of these variations have been presented in this section as tables and scatter plots for use in the design of terminal equipment of digital subscriber lines.

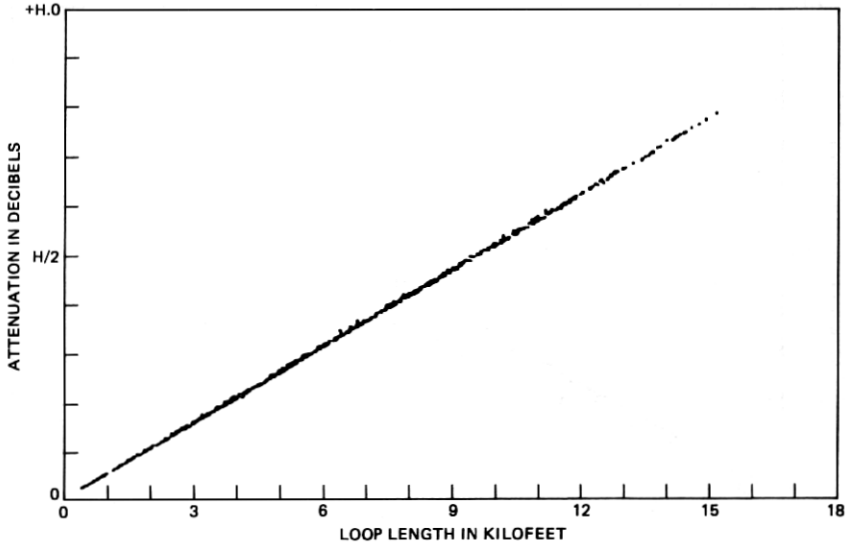

Fig. 3—Scatter plot of loop attenuations plotted against the equivalent loop length of No. 22 AWG cable. The frequency is 32 kHz and the temperature is 60°F. The X-scale is 2 kft/division and Y-scale is 5.0 dB/division.

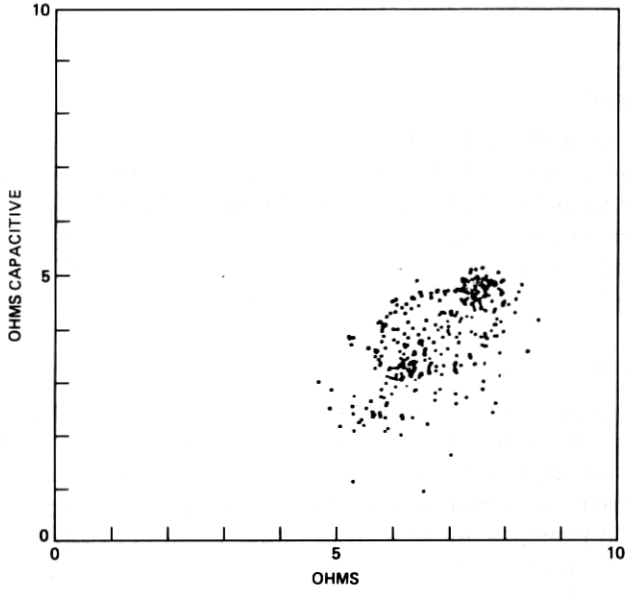

Fig. 4—Scatter plot of loop resistance plotted against its impedance (Central Office side). Temperature = 60°F, Frequency = 32 kHz, X- and Y-scales = 20 ohms/division.

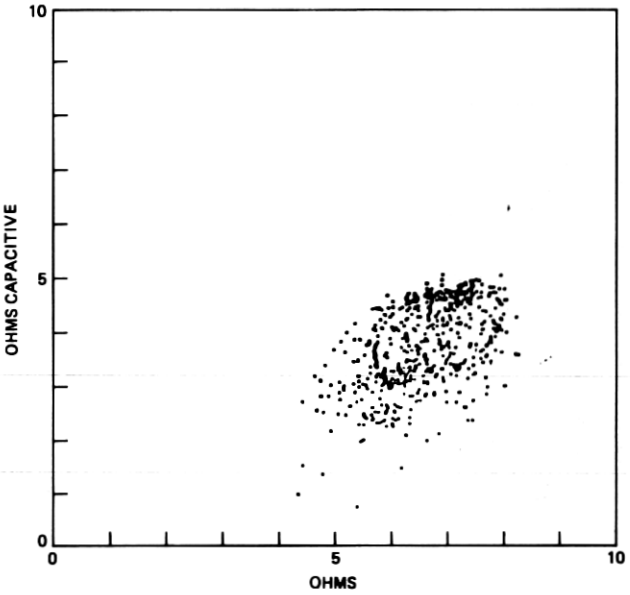

Fig. 5—Scatter plot of loop resistance plotted against its impedance (subscriber side). Temperature = 60°F, Frequency = 32 kHz, X- and Y-scale = 20 ohms/division.

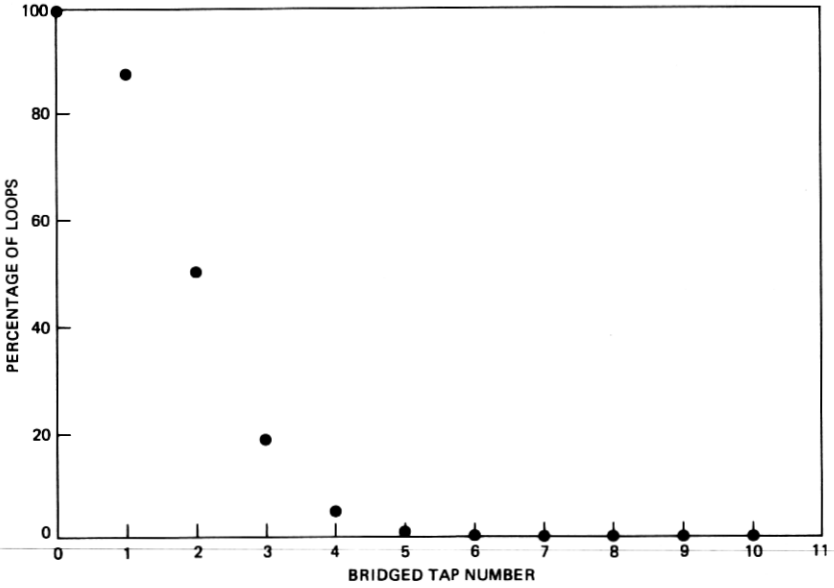

Fig. 6—Percentage of loops (Y-axis) having bridged taps equal to or greater than the bridged-tap number (X-axis) plotted.

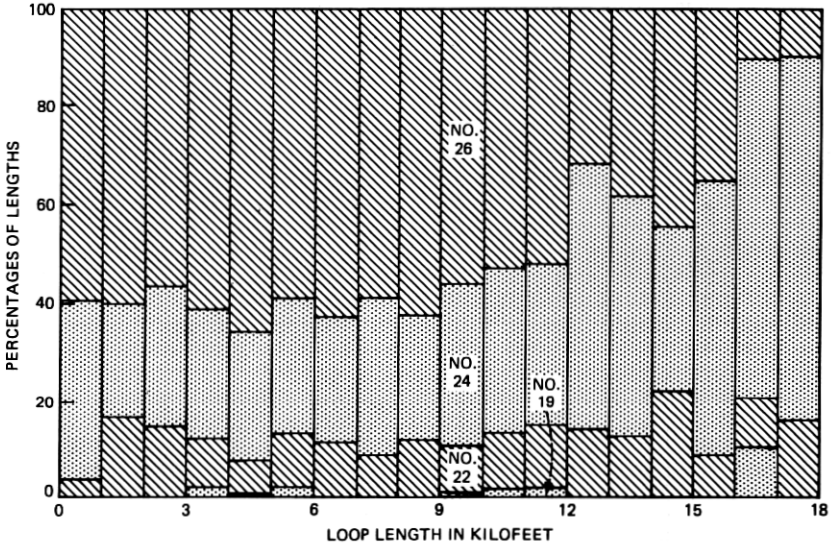

Fig. 7—Distribution of percentages of gauge sizes in the bridged taps.

IV. TIME-DOMAIN SIMULATIONS

4.1 Introduction

In this section, we present the time-domain results of typical hybrid data transmission systems, typical time-compression multiplexing systems with bipolar, ternary, partial response, and WAL-2 modes of coding. Single-pulse responses, pulse shapes, and eye diagrams are presented over a wide range of loop and terminating configurations.

The time-domain response of a transmission system is critically important in evaluating its capabilities to carry digital data. Such a response can be obtained from the spectral-domain response of the system by using conventional or fast Fourier transforms. However, FFTs were not used due to limited core capacity of the dedicated minicomputer on which the simulations were performed. The basis for obtaining the time-domain response of the entire system has been summarized in Section II.

4.2 Performance of the computational model

The flexibility of the software system to permit the simulation of any linear system configuration has been indicated (see Section II). Here, a hybrid duplex system with two electronic terminations having two four-section, sixth-order loss equalizers, (with equalization tailored for each loop) has been simulated.

When the cable length is made vanishingly small, typical component

(especially filter) performances and the validity of the model may be verified. Further, the delay through the filters may also be accurately determined. To establish these facts, two results are presented.

In Fig. 8a, a sequence of random pulses is used to excite the system from the CO to the S side. Forty-eight pulse positions are plotted here. The first 16-pulse positions are shown in the top one-third of the figure (see the second horizontal line from the top). The second and third 16-pulse positions are plotted on the fourth and sixth lines of the figure. Also, the second (+1)-pulse position (20.83 μs)* after the start of the 48-pulse duration is the response of the first (+1) pulse at the transmitter end.

In Fig. 8b, the eye diagram corresponding to the pulse train in Fig. 8a is shown. There are seven lines constituting the eye diagram. The two outermost lines are formed by 0, 1, 0 and 0, −1, 0 transitions. The two intermediate inner lines are formed by −1, 1, −1 and 1, −1, 1 transitions, and finally the three innermost lines are formed by 1, 0, −1; −1, 0, 1; and 0, 0, 0 transitions of the pulses. A pulse diagram similar to that shown in Fig. 8b for the S-to-CO direction of transmission is also obtained.

4.3 Single-pulse response over loops

Single-pulse response is essential to judge the capabilities of the overall system. Three crucial results emerge from the single-pulse response study: the deterioration of the received pulse, the extent of the long decaying tails left behind by the pulse, and the magnitude and the shape of reflections of the sent pulse at the sending end. Component values affecting these responses can then be suitably adjusted if the results prove unsatisfactory.

Single-pulse responses from single and multiple sections have been routinely computed, examined, and verified. Typical results from a three-section composite cable loop are presented in Figs. 9a through 9d. The loop consists of 3133 ft of No. 26 AWG cable, together with 8367 ft of No. 22 AWG cable, in series with 1365 ft of No. 19 AWG cable. The long tail of the pulse (Fig. 9a) received at the S side indicates that the following pulses would be offset from their zero position because of the influence of prior pulses. Next, consider the shape of the reflected pulse (Fig. 9b) on the S side. There are three peaks embedded in this pulse shape, and the central peak being almost as high as the received pulse would be a source of severe interference. Unless the reflections are substantially cancelled out by an echo canceler (see Section 4.4), the eye diagram would be considerably distorted.

---

* The bit rate for this particular simulation is 144 kb/s, and the delay can be computed by measuring the distance of the peak of this pulse (+1) from the instant $t = 0$ at the left-hand corner of the figure for the first 16 pulses.

Next, examine Figs. 9c and 9d. Here, the problem is exaggerated because of the relative magnitude of the received and reflected pulses, the ratio of these being 1:2.84. If it is desired to keep the pulse distortion down to 5 percent of the received-pulse height, the minimum amount of cancellation for the reflected signal should be 35 dB. Advancing one stage further, the single-pulse response can also predict that the nature of interference from a bipolar-pulse sequence 1, −1, 1, −1 is going to be different from the nature of interference caused by a pulse sequence 1, 0, 0, −1. In the former case, the positive half of the reflected pulse tends to become additive to the leading negative reflection of the next pulse, thus increasing the demands on the cancellation to about 41 dB. In the latter case, the reflections do not become additive because of the intermediate zeros in the pulse sequence. Similar considerations exist for the many different coding algorithms that can be used for transmission.

4.4 Random-data response

Random-data responses have been routinely generated to test the capability of the system over numerous loops. For the sake of consistency, results from the simulation of the loop in Section 4.3 are presented under this type of excitation. A random-pulse sequence of 48 bits is generated by selecting random bits of random numbers generated by the computer.

Further, we have been able to document excellent correspondence between computed eye diagrams and those from experimental results over a large number of loop configurations and bit rates. An example of this correspondence is evident between Figs. 10a and 10b. The experimentally generated eye (Fig. 10a) is obtained by transmitting 144-kb/s data over 18 kft of No. 22 AWG cable with 35 dB of echo cancellation (see Section 2.5). The eye opening is 74.7 percent. The computationally generated eye (Fig. 10b) is also obtained for the same conditions, and the eye opening is 74.8 percent. The eye opening is defined as the average of the top and bottom eye openings as a percentage to the average of the top and bottom eye heights.

4.4.1 Bipolar coding (hybrid transmission)

In the hybrid mode of transmission, the quality of the eye diagram depends on the extent of echo cancellation. To illustrate this point, Fig. 11a shows the eye diagram at the CO side of the loop, with no echo cancellation at 144-kb/s on a typical loop (3133 ft, No. 26 AWG; 8367 ft, No. 22 AWG; and 1365 ft, No. 19 AWG cables). Figure 11b shows the eye with perfect echo cancellation. Finally, Fig. 11c, shows an eye diagram with 30-dB echo cancellation.

4.4.2 Bipolar coding (time-compression multiplexing)

The transmission rate is increased to 324-kb/s for an effective bidirectional rate of 144 kb/s. The eye diagrams in this mode of operation are obtained by suppressing all reflections in the frequency domain, since only a unidirectional flow of data is present at any one instant. Figure 12 shows the eye diagram at the CO side of the loop.

4.4.3 Ternary coding

Simulations of ternary coding were limited because of the increasing degradation of the eye diagram. Most of the eyes were closed with composite cable loops and, hence, the results from a loop with 18 kft of No. 22 AWG cable, with 100 percent echo suppressions are given in Figs. 13a and 13b. Because of the symmetry of the loop, the corresponding figures for the other side of transmission are substantially the same as those in Figs. 13a and 13b; however, minor differences because of changes in clusters of bit patterns in the two 48-bit sequences (one from the CO side to S side and the other from the S side to CO side) are present. The ripple between bits $-1, -1, -1, \cdots$ and $1, 1, 1, \cdots$ was primarily responsible for the thickening of the eye in Fig. 13b. Further, long tails are also observed at the end of a sequence of data.

4.4.4 Class four partial response coding

Class four partial response coding[16] yields wave shape and eye diagram (Figs. 14a and 14b) considerably different from those with bipolar coding. Two distinct degradations occur. In the Y direction, the eye opening relative to the peak tends to suffer more because of the relative displacement of the peak of the eye relative to the peak eye opening. In the X direction, the horizontal eye opening tends to become limited because of the limited response of the system—the major advantage being that the system bandwidth is about one-half the bandwidth for bipolar coding. The particular loop over which the data transmission was simulated does not have any bridge taps but is composed of three cable sections as discussed in Section 4.3.

4.4.5 The WAL-2 codes

The WAL-2 codes also limit the bandwidth necessary for transmission.[17] The received data wave shape and eye diagram (Figs. 15a and 15b) also differ from those with the earlier types of codes. Here, the limited system response generates slowly varying pulse shapes (Fig. 15a). Generally, these codes are robust-to-line discontinuities but suffer in the presence of bridged taps. For the simulations given here, the loop was approximately 11 kft long, with nine cable sections and three bridged taps.

4.5 Time-compression multiplexing results with modified terminal configurations

The equalizer used for simulations in Section 4.4 has the capability to be tailored to the line loss by cascading up to three sections of sixth-order equalizers. Each of these sections provides for the loss of about 6000 ft of No. 22 AWG cable at 144 kHz. However, this particular approach has been abandoned in favor of an extended range equalizer (see Section 6.5). The circuitry for this equalizer has been adjusted such that there is a clear match between the attenuation of cables at different frequencies and the corresponding equalizer gain. Next, to simplify the termination impedance, the matching circuitry is substituted by a single resistance, which approximates the statistical average of the loop impedances at half the baud rate (see Table I, Section III). Further, it has been computationally determined (and experimentally verified) that the harmonics of the transmitted signal can be adequately controlled by adjusting the pulse width and, thus, saving the cost of an additional filter. Hence, the time-compression multiplexing simulations differ from the hybrid system to the extent that

(*i*) the bit rate is 2.25 times the bidirectional hybrid transmission bit rate,
(*ii*) the echo cancellation function is absent in the TCM mode,
(*iii*) the initial filtering of transmitted pulse is eliminated,
(*iv*) the pulse width has been computationally optimized at about 40 percent of the pulse period, and
(*v*) the matching circuit for all the cables has been approximated as the statistical average of all the resistive components of the image impedance of the cables at a frequency equal to half the baud rate.

The advantages of the hybrid system inherent in maximizing the bandwidth utilization and the impulse noise immunity have to be weighed against the complexity of the echo canceler necessary to eliminate the reflections and also against the enhanced NEXT interference (over that in the TCM system) into other cable pairs. Conversely, the simplicity of the design and construction of the time-compression multiplex system has to be weighed against the higher loop losses and increased impulse noise susceptibility caused by increased bandwidth.

In Figs. 16a and 16b, the experimentally and computationally generated eye diagrams are compared for 14 kft of No. 24 AWG loop at 324 kb/s. The eye opening predicted by the simulation is 85 percent, and the experimentally determined eye opening is 83 percent at an instant t_1, and is 76 and 75 percent, respectively at instant t_2. Similar results are obtained for typically mixed cable composition in Figs. 17a and 17b for a loop consisting of four sections. The No. 19 AWG cables at the

end of the loop make the configuration close to the worst type of cable composition. The experimentally determined eye opening is approximately 54 percent and the computationally predicted eye opening is 57 percent.

4.6 Effects of bridged taps

Bridged taps play a critical role in judging the capability of existing loops to carry digital data. At a particular bit rate, the number, lengths, and location of taps influence the pulse shapes and, consequently, the eye diagrams. For the simulation presented in this section, a No. 22 AWG, single-cable 10.5-kft loop with perfect echo cancellation is used. The results of the simulation are presented in Figs. 18a through 18d for zero-, one-, two-, and three-bridged taps, respectively. In Fig. 18a, there are no bridged taps on a 10.5-kft, No. 22 AWG loop. The bit rate is 144 kb/s, with perfect echo cancellation for all the simulations. In Fig. 18b, one bridged tap (No. 22 AWG, 1.5 kft long) is added 2 kft away from the CO end of the loop. In Fig. 18c, a second bridged tap (No. 22 AWG, 1.5 kft long) is added 1.5 kft away from the first bridged tap. In Fig. 18d, a third bridged tap (No. 22 AWG, 1.5 kft long) is added 1.5 kft away from the second bridged tap. The CO-to-S side eye diagrams for the four cases* are shown.

The results for other gauge cables are similar, but the results for composite cables with bridged taps are dramatically inferior to those presented here because of mismatch (and hence, additional eye closure) between the loops and terminating impedances.

4.7 Effects of pulse widths

Harmonic content of the transmitted signal may be controlled by filtering delta function excitation pulses or by altering the pulse width of the transmitted signals. The TCM system is a special beneficiary of the latter method (thus reducing the cost of an additional filter) because of the absence of received data during transmission. This makes the system more robust against NEXT interference (if the transmission and reception of data is synchronized).

The effect of changing the pulse width was studied with a particular TCM system. The simulation was carried out on a 17,314-ft eight-section loop from the 1973 loop survey data base. The composition of the loop is 7789 ft of No. 26 AWG; 2998 ft of No. 24 AWG; 2564 ft of No. 26 AWG; 25 ft of No. 24 AWG; 957 ft of No. 26 AWG; 2120 ft of No. 24 AWG; 141 ft of No. 26 AWG; and 720 ft of No. 24 AWG cables. From our experience, this particular loop had the worst eye opening carrying

* Overall optimization in the system design yields significantly better eye openings (see Sections VI and VII) in spite of bridged taps. In this Section, eye degradations caused by bridged taps in one of the early systems is shown.

324-kb/s data at 60°F in the TCM system. The results of changing the pulse width are shown in Fig. 19, showing a broad insensitivity to pulse width in the 20- to 40-percent duty cycle range for the particular equalizer simulated. This test has prompted the use of 40-percent duty cycle in the subsequent TCM simulations.

4.8 Conclusion

Simulations of the two general configurations for the bidirectional digital line have been accomplished. The system of time-domain programs is capable of simulating most of the physical conditions that exist on loops. Effects of temperature, code variations, component tolerances, and loop configurations on the eye diagrams have been routinely analyzed. Proposed systems are entirely simulated, and the effectiveness of each component on the eye opening is individually or combinatorially determined. The presence of bridged taps and their

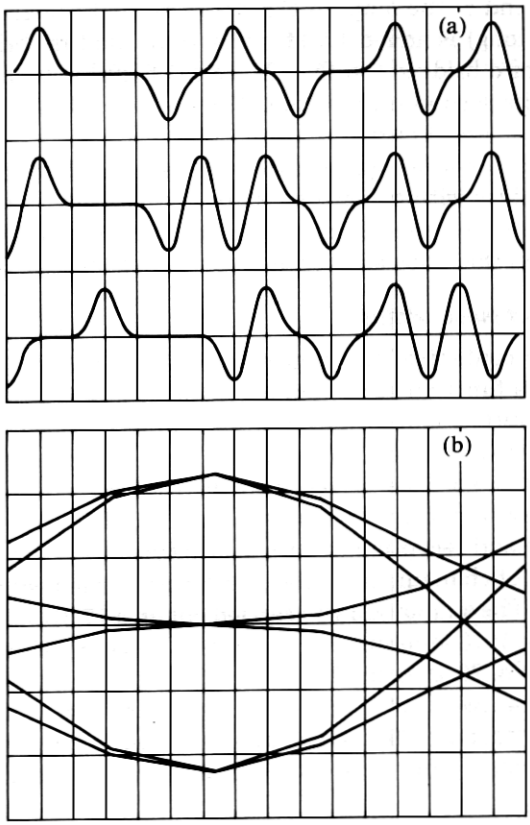

Fig. 8—System characteristics with zero loop length. (a) Pulse pattern and shape at the receiver. (b) Eye diagram at the receiver.

critical location in the loops is analyzed by a series of simulations. Crosstalk and impulse noise effects are not included in the simulation reported here.

The execution time of the programs has been about 20 minutes on a Data General Nova 2 minicomputer and about 50 seconds on a Data General Eclipse S-250 computer. It also translates to about 10 seconds on the IBM 370.

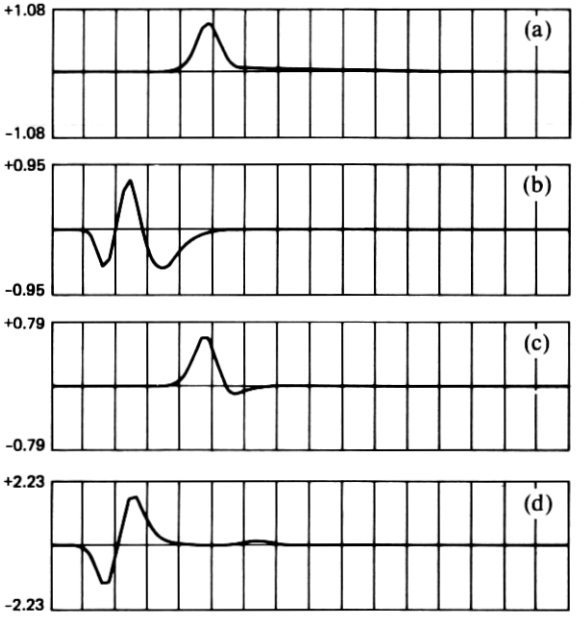

Fig. 9—Transmission and reflection of a single pulse on a typical loop consisting of three cable sections. Pulse rate is 144 kb/s, and each box width corresponds to 1-pulse duration. (a) Received pulse at S end of loop. (b) Reflected pulse at S end of loop. (c) Received pulse at CO end of loop. (d) Reflected pulse at CO end of loop.

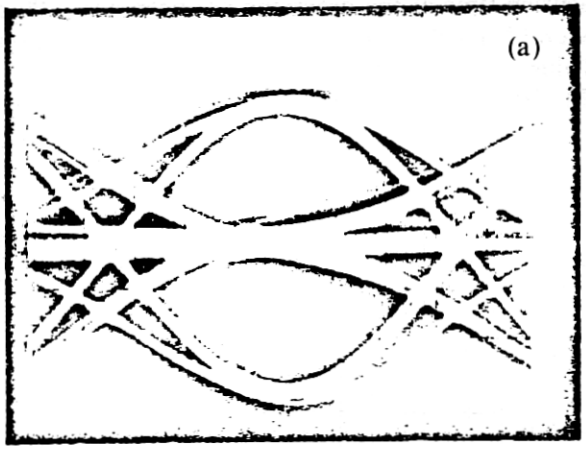

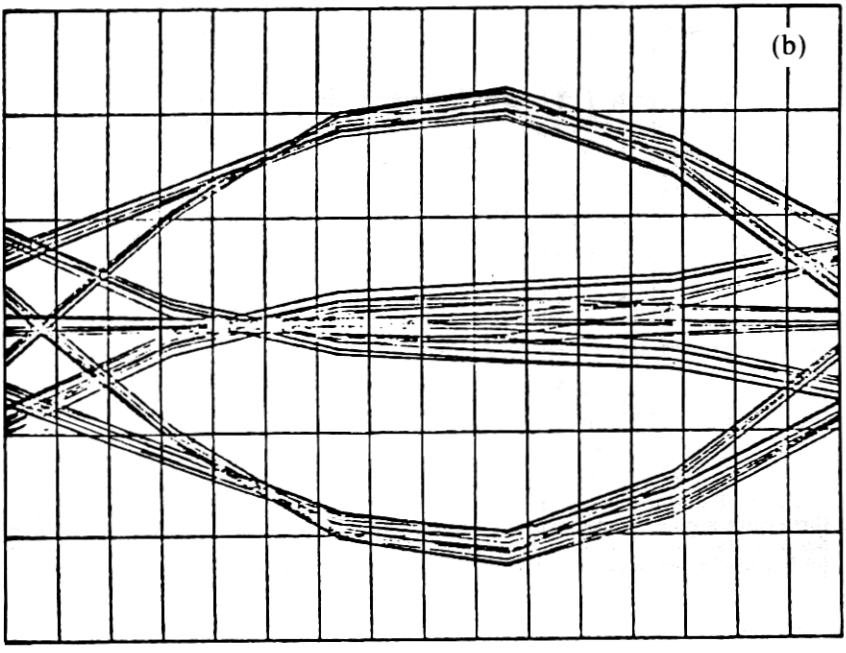

Fig. 10—Experimentally (a) and computationally (b) generated eye diagrams by transmitting bidirectional data over 18 kft of No. 22 AWG cable. The echo cancellation is 35 dB.

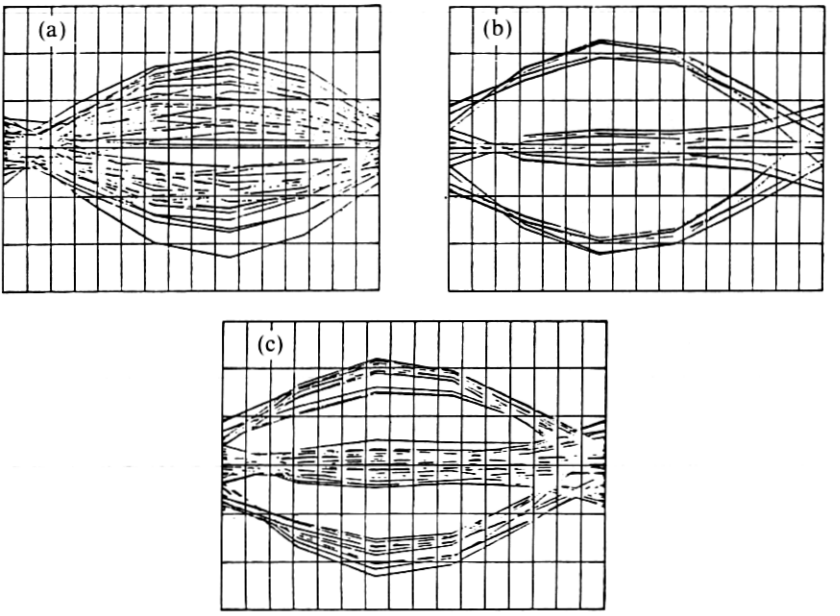

Fig. 11—Eye diagrams obtained by transmission of 144 kb/s bidirectional data over a typical loop. In (a) there is no echo cancellation, in (b) there is perfect echo-cancellation, and in (c) there is 30-dB echo cancellation.

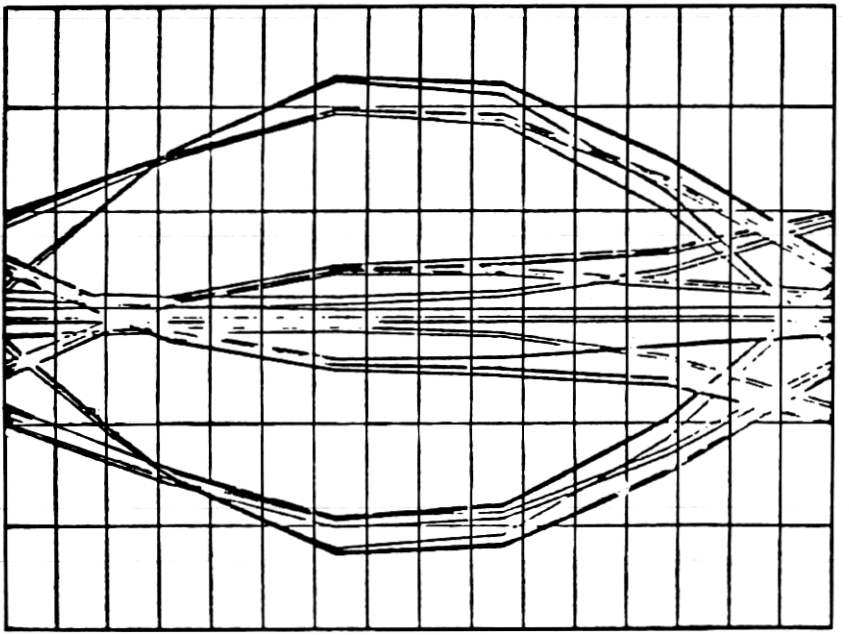

Fig. 12—Eye diagram obtained by transmission of data at 324 kb/s (for an effective bidirectional rate of 144 kb/s) in the TCM mode. The loop configuration is the same as that for the simulations in Fig. 11.

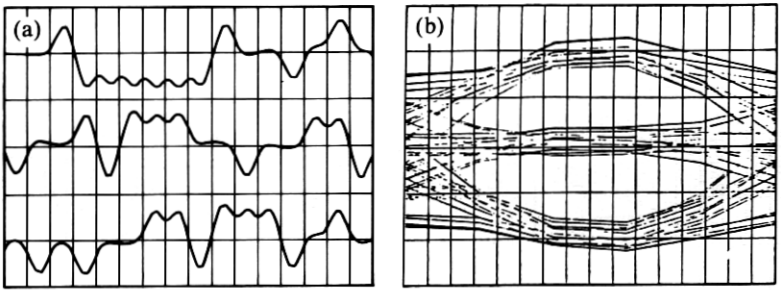

Fig. 13—Pulse pattern and eye diagram obtained by ternary code at 144 kb/s. The loop is 18 kft of No. 22 AWG cable. (a) Subscriber-side pulse pattern. (b) Subscriber-side eye diagram.

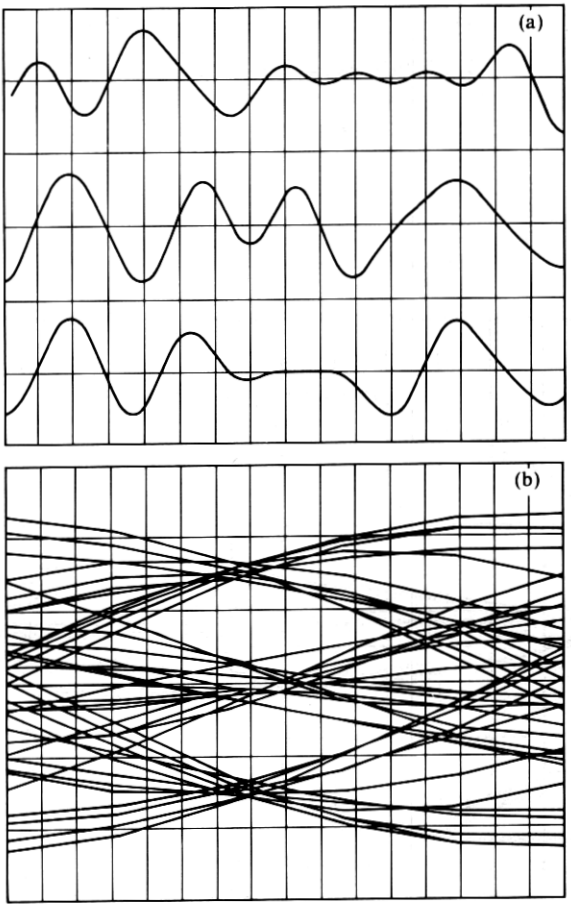

Fig. 14—Pulse pattern and eye diagram obtained by class four partial-response coding. The loop is a typical three-section loop, and the bit rate is 144 kb/s. (a) Subscriber-side received data. (b) Subscriber-side eye diagram.

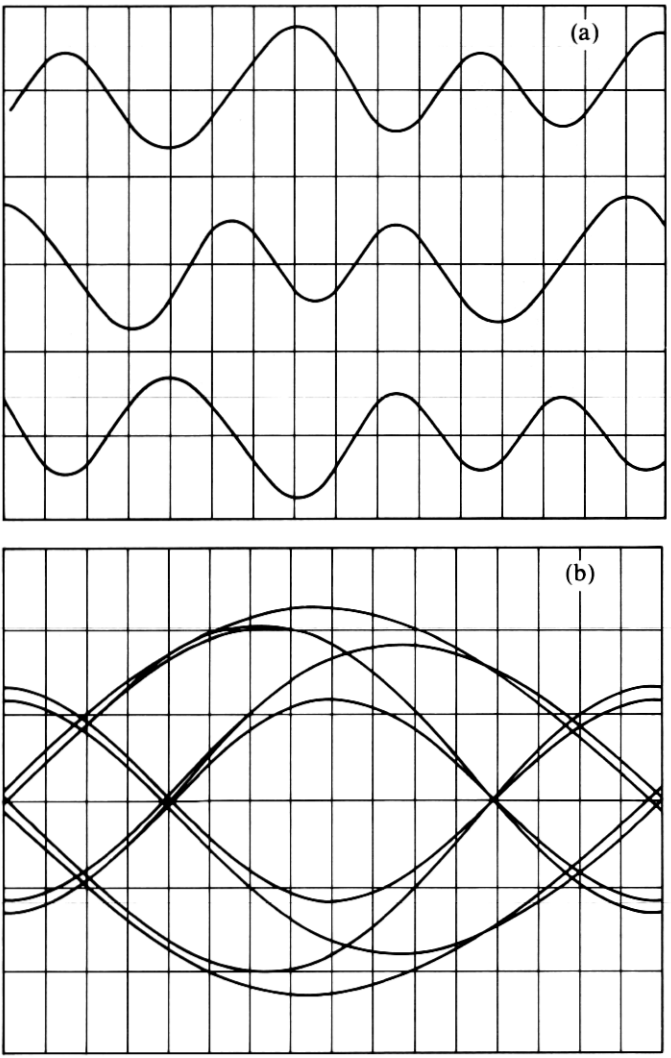

Fig. 15—Pulse pattern and eye diagram obtained by WAL-2 code. The loop configuration has nine cable sections and three bridged taps, and the bit rate is 144 kb/s. (a) Subscriber-side received data. (b) Subscriber-side eye diagram.

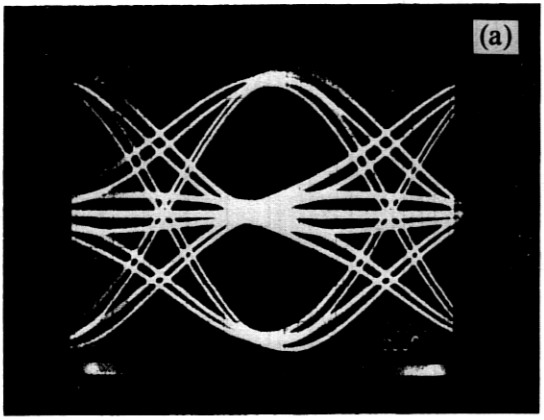

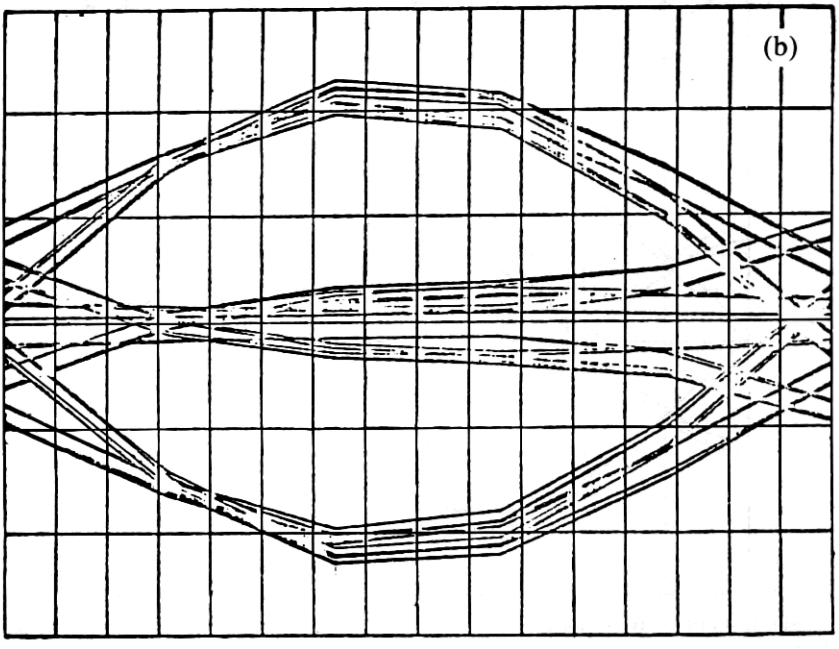

Fig. 16—Experimentally (a) and computationally (b) generated eye diagrams over 14 kft of No. 24 AWG cable. The bit rate is 324 kb/s, and the half-bit rate loop attenuation is approximately 39 dB.

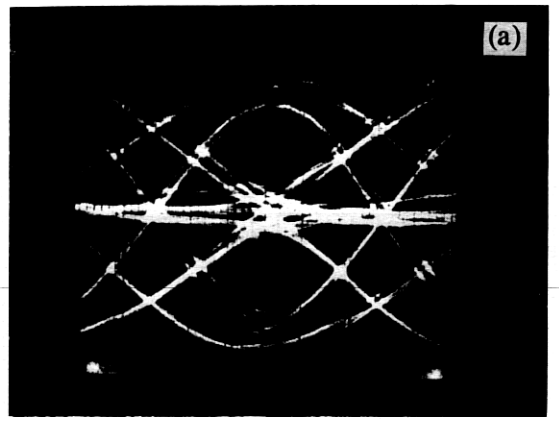

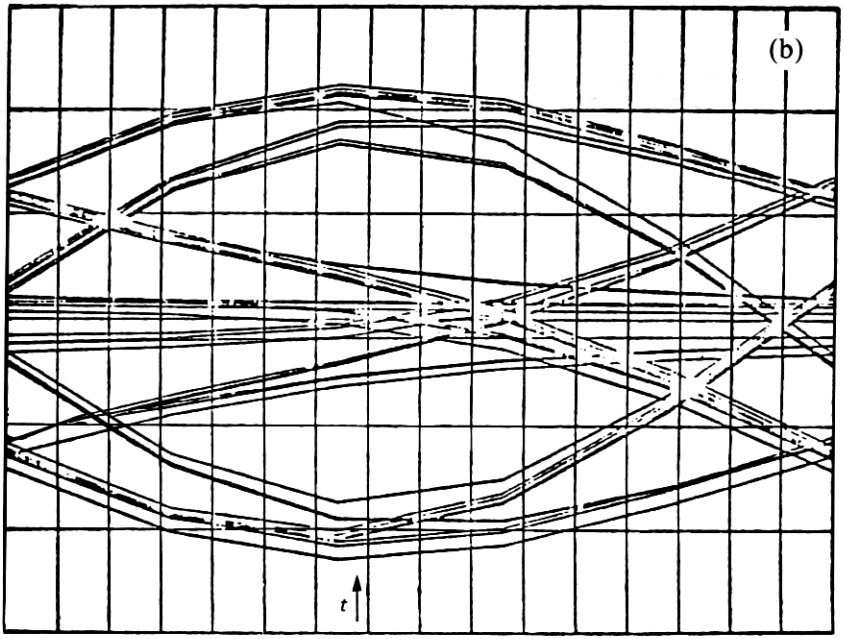

Fig. 17—Experimentally (a) and computationally (b) generated eye diagrams over a four-section (3.46 kft, 19 AWG; 8.7 kft, 24 AWG; 9.8 kft, 22 AWG; 3.46 kft, 19 AWG) loop at 324 kb/s in the TCM mode. The loop attenuation at half-bit rate is approximately 48 dB.

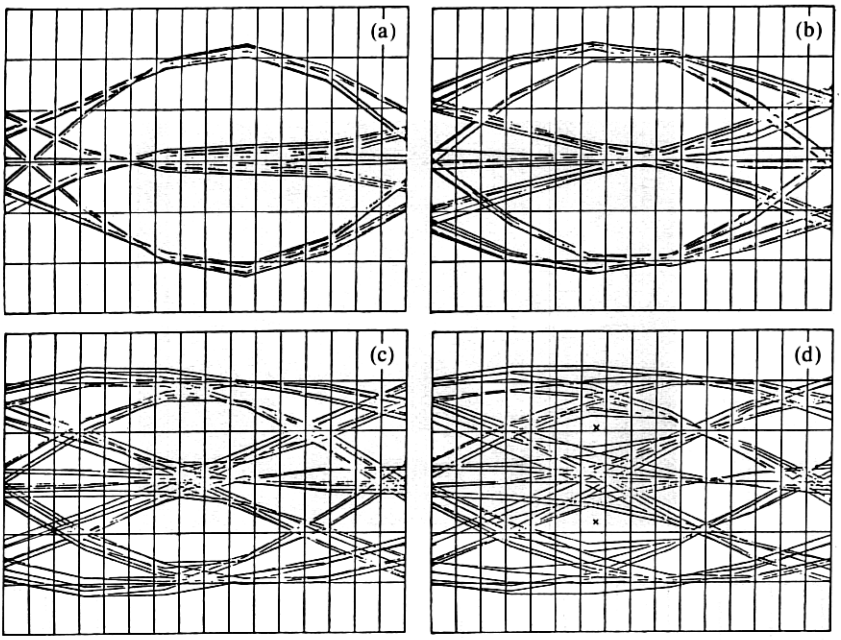

Fig. 18—Degradation of the eye diagram with an increasing number of bridged taps. (a) Subscriber-side eye diagram, no bridged taps. (b) Subscriber-side eye diagram, two bridged taps. (c) Subscriber-side eye diagram, two bridged taps. (d) Subscriber-side eye diagram, three bridged taps.

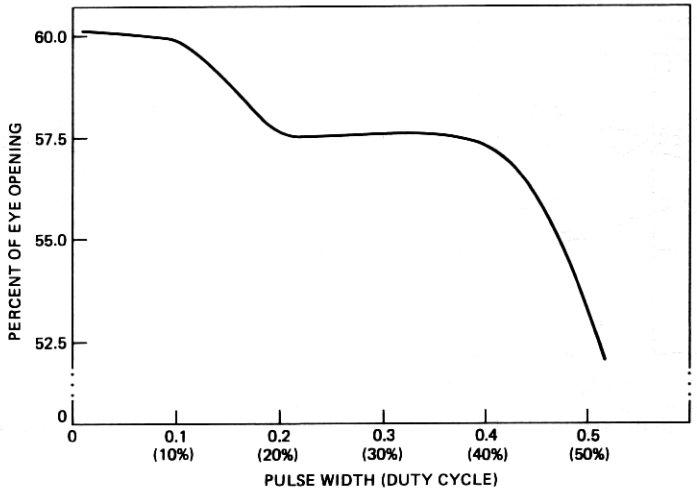

Fig. 19—Effect of varying the pulse width on the eye opening of 17,314-ft loop composed of eight discrete cable sections with a typical equalizer (see Section 5.5).

V. SUMMARY OF 1973 LOOP SURVEY SIMULATIONS UNDER VARIOUS TERMINAL CONFIGURATIONS

5.1 Introduction

The time-domain simulations yield pulse shapes and eye diagrams. The loop plant, however, consists of a widely diverse collection of loops (see Section III). Thus, we have been able to establish a computational link between the simulation programs and the loop survey data base such that the program systematically simulates the data transmission with any prescribed terminal configuration loop by loop on a statistically significant population of the Bell System loops.

5.2 From eye diagrams to eye statistics

Two hundred and forty equally spaced instants of time span the 48-pulse period over which the 48 random binary pulse data are transmitted. Hence, the pulses are approximated as a sequence of five straight lines (in the time domain). Out of the 240 instants of time for scanning 48 ones, zeros, or minus ones, 144 instants are selected for the scanning of the 48 data bits. The first set of 48 instants contains the instant at which the absolute maximum value of the incoming magnitude is located. The second set of 48 instants precedes the first 48 instants by one-fifth the pulse duration, and the third set follows the first 48 instants by one-fifth the pulse duration.

Next, for each of the three sets of 48 instants at which the scanning can be done, the data are arranged in diminishing order of magnitude. Three clusters of data are generated: (*i*) at the upper level, corresponding to the plus ones received in the data; (*ii*) at the intermediate level, corresponding to the zeros received; and (*iii*) at the lower (minus) level, corresponding to the minus ones received. From these three clusters seven eye statistics can be generated. In Fig. 20, the three scanning instants t_1, t_2, and t_3, and the five data clusters, representing the distances a_ib_i, b_ic_i, c_id_i, d_ie_i, and e_if_i ($i = 1$, 2, or 3), are indicated. Next, a_ib_i expressed as a proportion of the average eye height constitutes the top eye thickness, b_ic_i, c_id_i, d_ie_i, and e_if_i, also expressed as proportions of the average eye height, constitute the top eye opening, the central thickness, the lower eye opening, and the bottom eye thickness, respectively. Finally, the positive average eye height and negative average eye height constitute the sixth and seventh pertinent eye statistics from the eye diagram at each of three scanning instants t_i ($i = 1$, 2, or 3). However, the scanning instant t_i is selected to have the maximum average top and bottom eye opening leading to a unique scanning instant and a unique set of seven statistics stored away for each eye. Two such seven-parameter, eye-statistical sets for each of the two eyes generated by data from CO to S and from S to CO are thus stored for each loop.

5.3 From eye statistics to scatter plots

The eye statistics of loops in the data base are generated and stored under a predefined set of terminal conditions. These eye statistics can now be displayed as a collection of scatter plots, each dot denoting a particular eye statistic of a particular loop. The top and bottom eye-opening statistics are assembled in one scatter plot. Along the X-axis, the physical length of the loop or the equivalent length of No. 22 AWG cable (or, equivalently, the loop attenuation) may be plotted. The top central and bottom eye thickness may also be plotted on one scatter plot. With two independent directions of transmission, a set of eight scatter plots are obtained for each transmission scheme. The next set of plots is obtained by separating out the loops by the number of sections. Here, the X scale is plotted by the length of the loop but compressed by two-thirds to accommodate loops in the (1, 2, 3), (4, 5, 6), or ($\geq$7) sections and up to 18,000 ft on each plot. A typical example of the entire set consists of 24 scatter plots. Here, we present six such plots (Figs. 21a through 21f) obtained by transmitting data at 80 kb/s in the TCM mode at line rate of 180 (2.25 $\times$ 80) kb/s. In Fig. 21a, the loop length is shown on the X-axis. The eye thickness (see Section 5.2) data are plotted in the Y direction. In Fig. 21b, the eye thickness is plotted against the equivalent length of the loop in kft of No. 22 AWG cable at 55°F. At half the bit-rate frequency of 90 kHz, each division indicates about a 3.3-dB loop loss. In Figs. 21c through 21e, the eye thickness data from three sets of loops with 1-, 2-, or 3-cable sections, 4-, 5-, or 6- cable sections, and finally 7-, 8-, or $\geq$9-cable sections are plotted.

To study the effect of the accuracy of equalization, we have generated the next family of scatter plots which indicates the eye height (also as a scatter plot), together with the eye opening and eye thickness data. In Fig. 21f, the effect of the eye height (which is allowed to change by approximately 20 percent by adjusting the equalization) on the eye thicknesses is plotted as scatter plots in the top half of the plots. In the lower half, the eye height data are plotted.

5.4 Worst loop tabulations

The scatter plots are a collection of points with each trio (Fig. 21f) or quad (Figs. 21a, etc.) representing a loop. However, it becomes necessary to identify the loops that do indeed cause failure or unexpected eye closures. For this reason, a set of programs has been developed which identifies and tabulates the loops whose eye openings lie between any two predefined percentages for any terminal configuration. For example, the composition of loops that have a $\geq$25 percent eye closure is shown in Table VI.

Table VI—Data of loop that exhibit more than 25 percent eye closure

```
  WORST LOOP SEARCH-LOOP DETAILS—
  EYE CLOSURE = 25 PERCENT
   130,  5,    26,  2,
  4671, 24,  5348, 22,   671, 26,  759, 19,  4122 22,
   199,  6,    30,  2,
  2512, 22,  2333, 24,  4238, 22,  573, 24,  7292, 22,  190, 24,
   456,  2,    29,  2,
 13643, 22,   724, 26,
   699,  3,    28,  2,
 13308, 26,  1412, 24,   990, 26,
   740,  2,    25,  2,
 11523, 22,  6224, 24,
   741,  8,    27,  2,
  7789, 26,  2998, 24,  2564, 26,   25, 24,   957, 26,  2120, 24,  141, 26,
   720, 24,
   765,  5,    29,  2,
 10694, 22,  1530 19,  1638, 24,  303, 26,  2477, 24,
R
```

Note: The first number (130) indicates the loop number, the second number (5) indicates the number of cable sections. The third and fourth numbers indicate the percentage eye closure (26) and the direction of transmission (2 for S to CO and 1 for CO to S). The number pairs on the next line denote the cable length and the gauge number. Five such numbers are printed because there are five cable sections. The same data format repeats for the next six loops.

5.5 Percentage failure analysis

An alternate way to investigate the success or failure of any terminal configuration is to identify the percentage of loops in each kilofoot band that has eye closure in excess of the prechosen eye openings. Typically, eight eye-closure (2.5, 5, 7.5, 10, 12.5, 15, 20, and 30 percent) limits are defined, and there are eighteen 1-kft bands in the loop data base. Results for the 80-kb/s TCM mode transmission is shown in Table

Table VII—Percentage of loops in each kilofoot band capable of carrying data with less than the specified eye closure (CO-to-S-data)

	Percentage (Eye Closure)							
	2.5	5	7.5	10	12.5	15	20	30
0–1	0.00	0.00	0.00	0.00	0.00	100.00	100.00	100.00
1–2	0.00	0.00	0.00	0.00	7.89	100.00	100.00	100.00
2–3	0.00	0.00	0.00	0.00	89.29	100.00	100.00	100.00
3–4	0.00	0.00	0.00	46.38	98.55	100.00	100.00	100.00
4–5	0.00	0.00	1.56	96.87	100.00	100.00	100.00	100.00
5–6	0.00	0.00	54.55	96.10	100.00	100.00	100.00	100.00
6–7	0.00	0.00	59.37	92.19	98.44	100.00	100.00	100.00
7–8	0.00	1.39	52.78	95.83	100.00	100.00	100.00	100.00
8–9	0.00	0.00	10.45	89.55	94.03	98.51	100.00	100.00
9–10	0.00	0.00	7.55	73.58	86.79	100.00	100.00	100.00
10–11	0.00	5.45	40.00	56.36	70.91	89.09	100.00	100.00
11–12	0.00	28.85	40.38	55.77	61.54	73.08	100.00	100.00
12–13	0.00	34.21	52.63	63.16	68.42	76.32	89.47	100.00
13–14	0.00	9.68	32.26	54.84	67.74	70.97	80.65	100.00
14–15	0.00	15.38	26.92	50.00	57.69	73.08	92.31	100.00
15–16	0.00	9.52	23.81	42.86	47.62	57.14	66.67	100.00
16–17	0.00	0.00	50.00	83.33	83.33	83.33	83.33	100.00
17–18	0.00	6.25	25.00	37.50	43.75	50.00	62.50	100.00

VII for the CO-to-S eye data. A totally perfect system would have a 100-percent result for each of the elements of the table, and a totally unacceptable system will have zeros for all the elements. Thus, the higher numbers toward the center of the table would tend to reflect the compromise in the designing terminal equipment and its cost. If the criterion is for 90 percent of the loop population to have 80 percent or better opening, the average of the number in the eighth column should be greater than or equal to 90, etc.

5.6 Simulation data for typical 64- and 144-kb/s TCM and hybrid system with and without bridged taps

Each simulation generates a large number of scatter plots and associated tables. This section gives the highlights of eight such simulations (Figs. 22 through 29). In Figs. 22a and 22b, the eye-opening and eye-thickness data for a 64-kb/s hybrid system are plotted with 30-dB echo cancellation. Figure 22 pertains to CO-to-S data transmission and similar results (Figs. 23 through 29) are given under the other conditions.

Table VIII—Loop percentage failure and shortest length for failure

Rate	Mode	No Bridged Taps	With Bridged Taps
64 kb	Hybrid	9.0%, 12 kft	31.2%, 5.7 kft
	TCM	0.0%, 18 kft	2.0%, 2.7 kft
144 kb	Hybrid	8.4%, 9 kft	46.5%, 2.5 kft
	TCM	0.0%, 18 kft	26.1%, 0.5 kft

5.7 Discussion of the simulation results

An example of the effect of bridged taps under a hybrid mode of transmission can be identified by comparing Figs. 22 and 23 at the 64-kb/s rate or Figs. 24 and 25 at the 144-kb/s rate. Similarly, the effect of bridged taps in the TCM mode of transmission is identifiable by comparing Fig. 26 with 27, or 28 with 29 at the two data rates. Conversely, a hybrid and a TCM system can be compared at the two rates by comparing Fig. 22 against 26, or Fig. 23 against 27 for the 64-kb/s rate, and by comparing Fig. 24 against 28, or Fig. 25 against 29 for the 144-kb/s rate.

5.7.1 An example of a comparison of a TCM system with a hybrid system

The entire population of loops in the loop survey can carry bidirectional data at 64 or 144 kb/s up to 18 kft with the TCM system when the bridged taps are stripped. The eye closure in all the cases has been computed to be <42 percent. In the hybrid mode with 30-dB echo

cancellation and with similar equalization, the failure rate (criterion: eye closure >40 percent) is expected to be 9 percent at 64 kb/s, when all the bridged taps are stripped, and climb up to 31.2 percent with the bridged taps intact.

At 144 kb/s with the TCM system, all the loops (no bridged taps) carry the bidirectional data with 40 percent or less eye closure, except one single loop which exhibits a 42-percent closure. Under similar conditions, the hybrid system with 30-dB echo cancellation yields a loop failure rate of about 8.4 percent. Bridged taps deteriorate the performance of both the TCM and the hybrid systems. However, the TCM system suffers a 26.1-percent loop failure against 46.5 percent for the hybrid system with 30-dB echo cancellation.

The next significant observation is that in the hybrid system at 64 kb/s with all the bridged taps stripped, the data can be transmitted successfully on all loops up to 12 kft, and the failure rate is 8, 35, 61, 76, 66, and 81 percent in each of the 1-kft bands up to 18 kft. At 144 kb/s-data transmission on the loops with all the bridged taps stripped is successful up to about 11 kft. The failure rates for 12- to 18-kft bands have been computed as 15.4, 26.3, 25.8, 7.7, 52.4, 66.7, and 100 percent, respectively.

Further, the effect of the bridged taps forces the limitations of the loop length to 5.7 kft at 64 kb/s in the hybrid mode and to about 2.1 kft at 144 kb/s. At 64 kb/s the failure rates in each of the 1-kft bands between 5 to 18 kft are 1.3, 1.6, 8.33, 61.2, 71.7, 72.73, 69.3, 63.2, 51.6, 73.1, 76.1, 66.6, and 81.25 percent, respectively. At 144-kb/s, only the 1- and 2-kft band qualify with a 100-percent success for data transmission, and loop failure with other sixteen 1-kft bands are 3.57, 1.45, 6.25, 23.38, 35.96, 26.39, 82.09, 88.68, 70.9, 73.1, 79.47, 100, 92.31, 95.24, 100, and 100 percent, respectively. On the other hand, the TCM mode of transmission is not particularly sensitive to loop length but, instead, to the particular bridged-tap length. The hybrid system suffers twice because of (*i*) reflection of the transmitted signals caused by impedance mismatches, and (*ii*) reflections from the bridged taps in the direct transmission path. The situation becomes complicated because of the length, number, and the distribution of the bridged taps along the loop length.

5.7.2 Comparison of results for loops without and with bridged taps

Loop failure is particularly susceptible to the presence of bridged taps. In the hybrid system at 64 kb/s, the penalty is that approximately 22 percent (from 9.0 to 31.2 percent) more loops become incapable of carrying the data. In the TCM system, about 2 percent (from 0.0 to 2 percent) loops are excluded. In the hybrid system at 144-kb/s, the penalty is about 38 percent (from 8.4 to 46.5 percent) of the loops

because of the presence of the bridged taps, whereas the TCM system suffers a 26 percent (from 0.0 to 26.1 percent) increased loop failure. These results are summarized in Table VIII. The next observation is that the loop-failure percentage has very little to do with the shortest loop that fails. Stated alternatively, the failure is likely to be independent of the loop length. However, from further analysis the characteristics of the failed loops indicate that even one single-bridged tap of critical length and appropriate gauge located anywhere along its length can destroy the eye. It has been determined that the length of this bridged tap is such as to cause a delay of one (or an integer number of) pulse period (periods, to lesser extent), thus, resulting in a systematic obliteration of the eye from either direction.

The former observation is further confirmed by the fact that the shortest loop length (Table VIII) for a 144-kb/s TCM system is only 0.5 kft, whereas the loop percentage failure is about 26 percent. Similar results for the hybrid system indicate that the shortest loop length is about 2.5 kft, and the percentage failure rate is about 46 percent.

5.8 Summary of results and conclusions

We have been able to obtain the overall performance of many systems under different terminal conditions. The results presented in this paper are based on an equalizer (Section VI). In the hybrid mode of data transmission, there is reason to conclude that deterioration

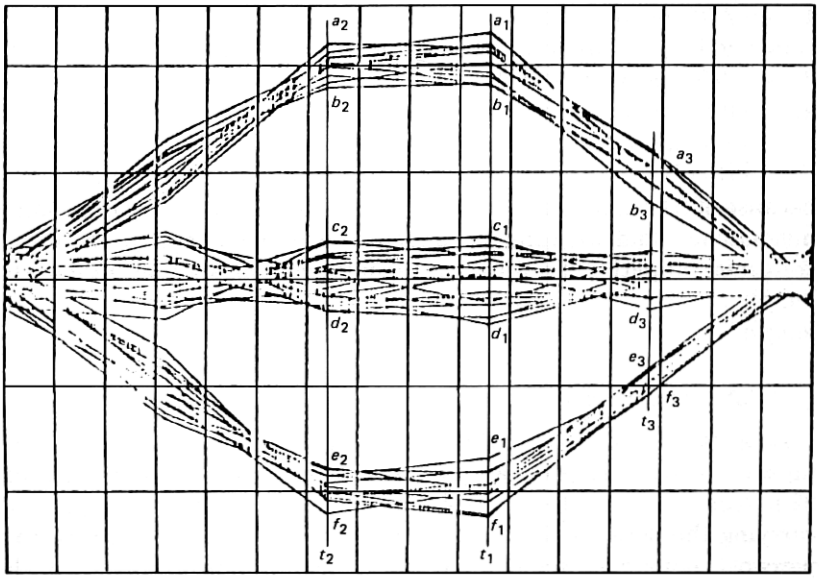

Fig. 20—Extraction of eye statistics from the eye diagram.

starts to become worse after the shortest loop length for failure is reached, whereas a similar conclusion is not evident in the TCM mode. In the former case, the eye deterioration is basically caused by (*i*) reflections, and (*ii*) delayed transmissions. While the signal strength starts to fall because of longer loop lengths, the reflected signal retains

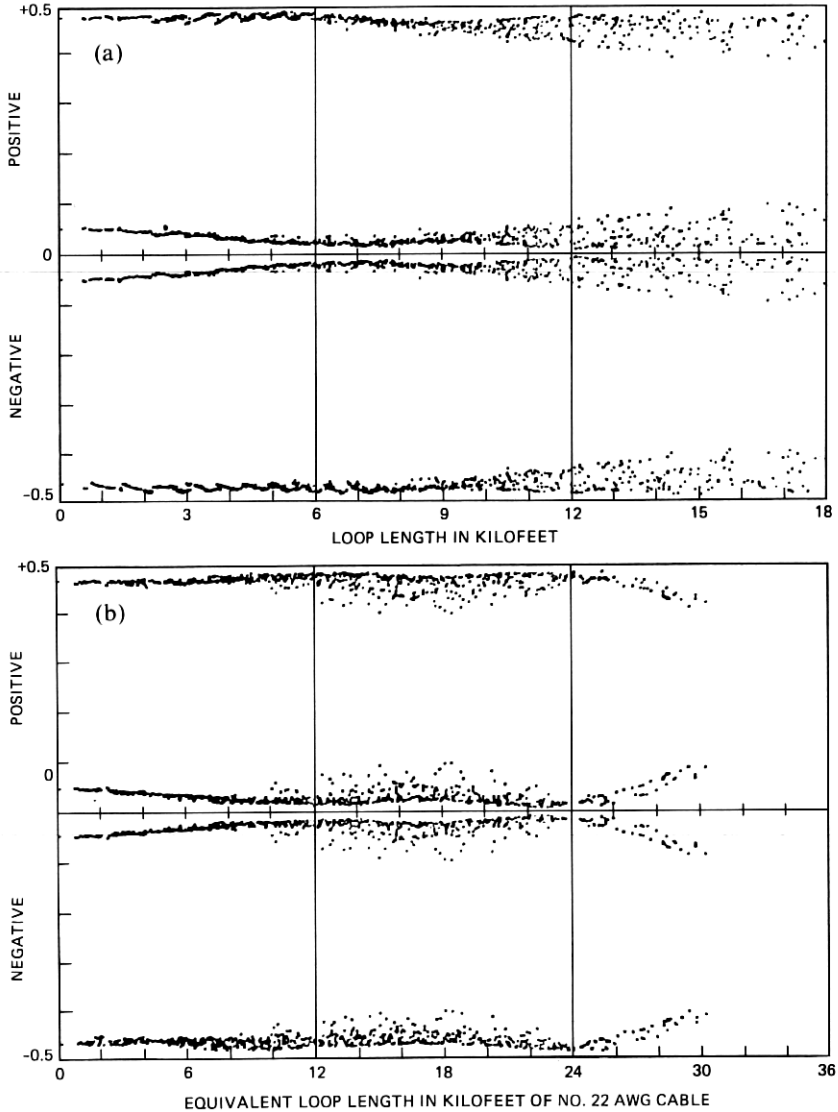

Fig. 21—Eye thickness scatter plots for 80-kb/s data transmission in the TCM mode. In the set of six figures (a through f) the data at the s end of the loops are given. (a) Eye thickness (*Y*-axis) versus loop length in kft (*X*-axis). (b) Eye thickness versus equivalent loop length (expressed in kft of No. 22 AWG cable).

its strength. The delayed transmission, which is of concern to both the hybrid and the TCM mode, can interfere with the pulse in the next time slot. In the TCM mode, the delayed transmission alone is the cause of loop performance degradation.

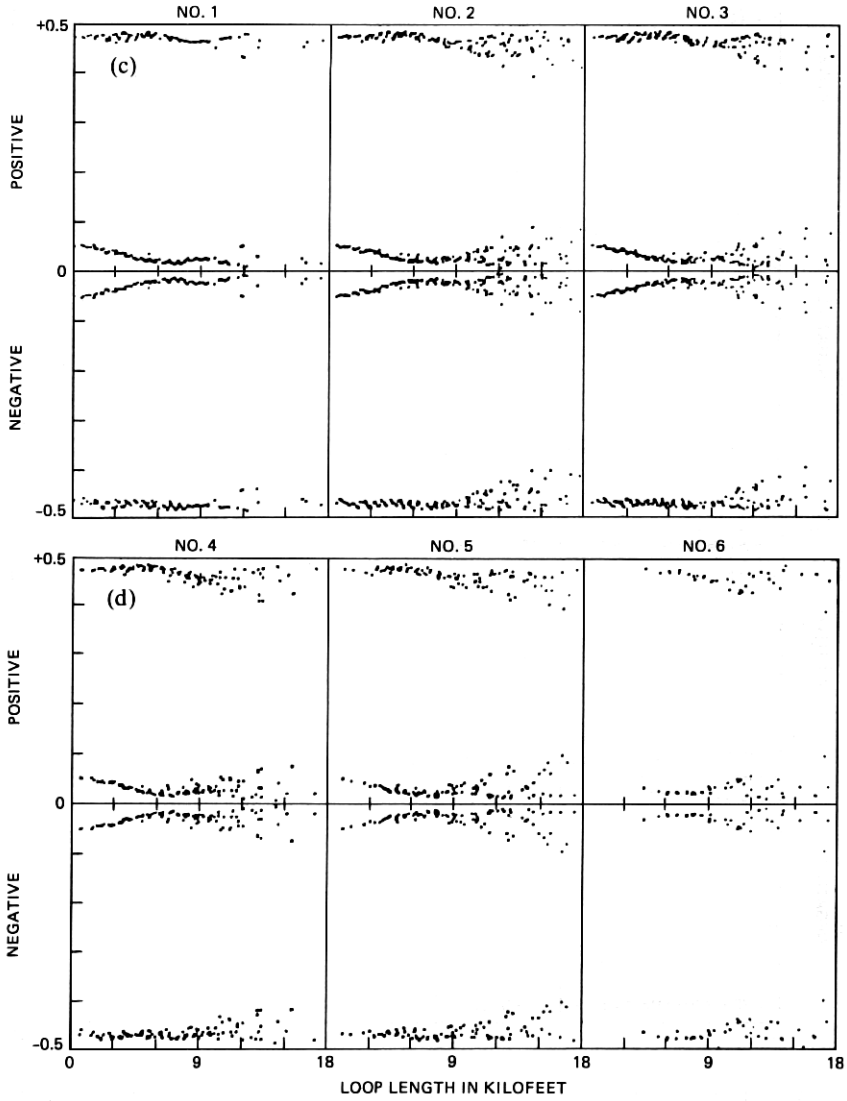

Fig. 21—(c) Eye thickness for loops with 1-, 2-, or 3-cable sections versus loop length in kft (numbers indicate number of sections). (d) Eye thickness for loops with 4-, 5-, or 6-cable sections versus loop length in kft (numbers indicate number of sections).

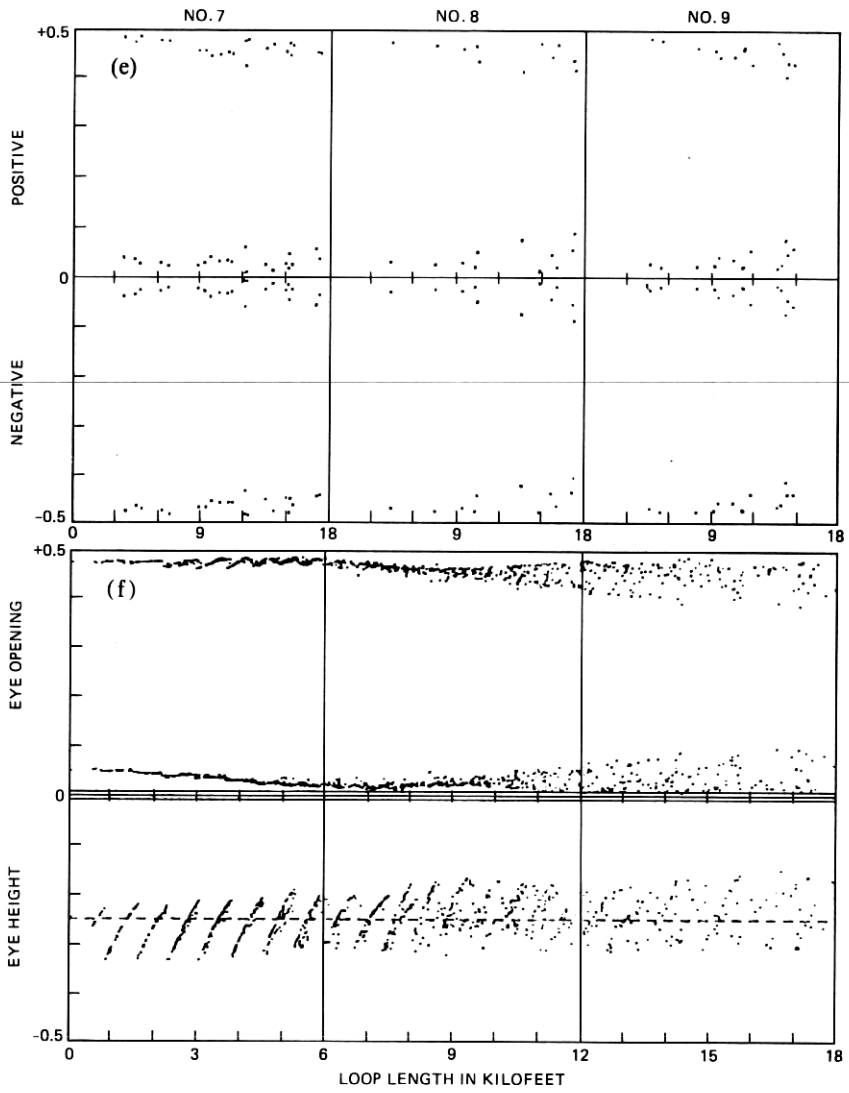

Fig. 21—(e) Eye thickness for loops with 7-, 8-, or ≥9-cable sections versus loop length in kft (numbers indicate number of sections). (f) Eye thickness and eye height for all loops versus loop length in kft.

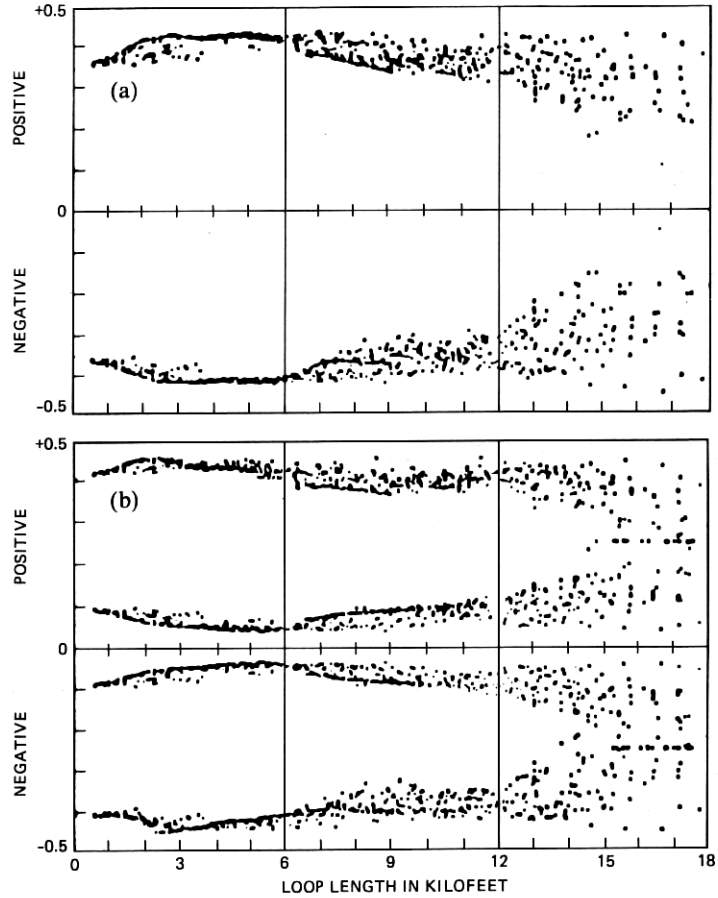

Fig. 22—Eye data scatter plots for 64-kb/s hybrid transmission with 30-dB echo cancellation. Bridged taps are stripped from the loops. Subscriber side data are given. (a) Eye opening. (b) Eye thickness.

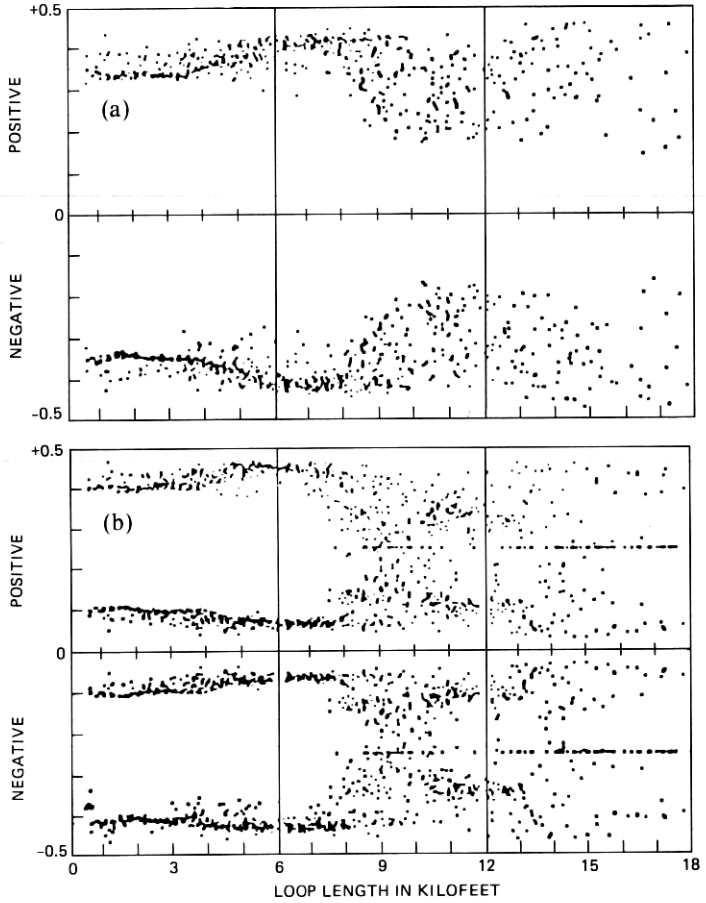

Fig. 23—Eye data scatter plots for 64-kb/s hybrid transmission with 30-dB echo cancellation. Bridged taps are left intact. Subscriber side data are given. (a) Eye opening. (b) Eye thickness.

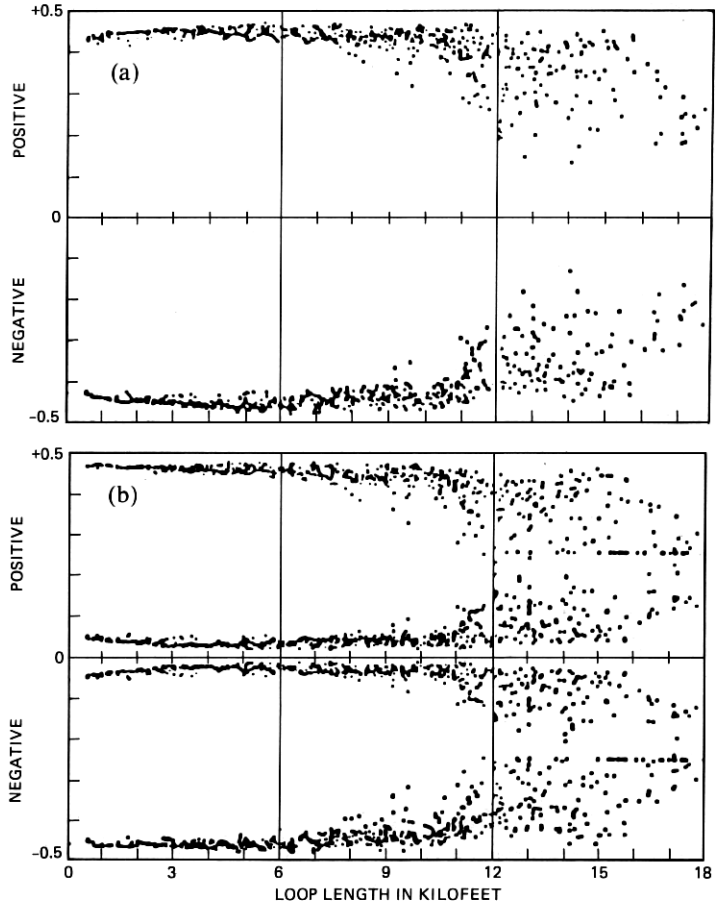

Fig. 24—Eye data scatter plots for 144-kb/s hybrid transmission with 30-dB echo cancellation. Bridged taps are stripped from the loops. Subscriber side data are given. (a) Eye opening. (b) Eye thickness.

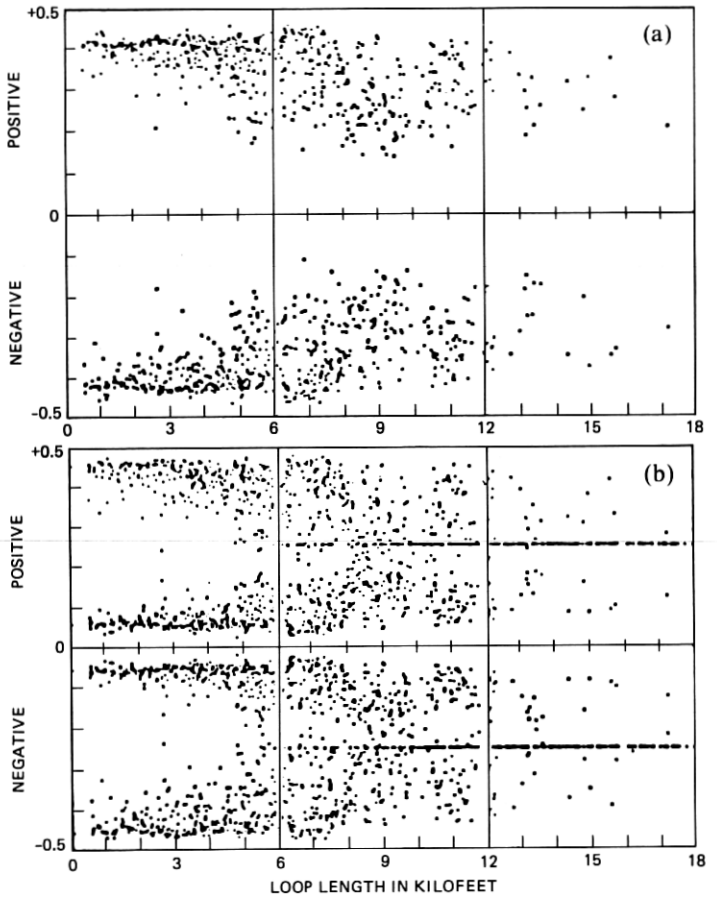

Fig. 25—Eye data scatter plots for 144-kb/s hybrid transmission with 30-dB echo cancellation. Bridged taps are left intact. Subscriber side data are depicted. (a) Eye opening. (b) Eye thickness.

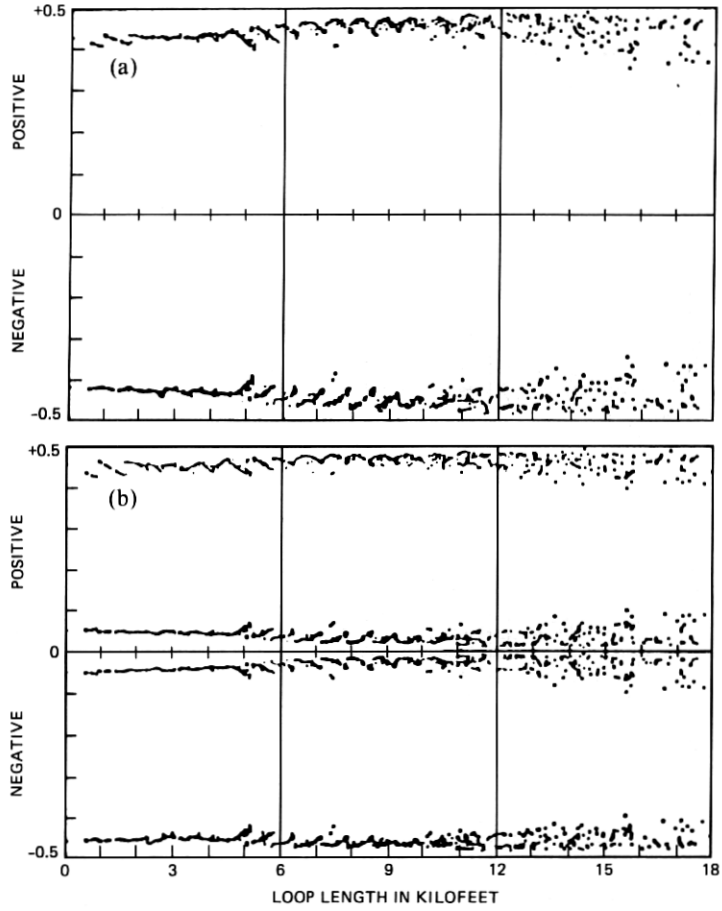

Fig. 26—Eye data scatter plots for 64-kb/s TCM-mode transmission (actual line rate is 144 kb/s). Bridged taps are stripped from the loops. Subscriber side data are given. (a) Eye opening. (b) Eye thickness.

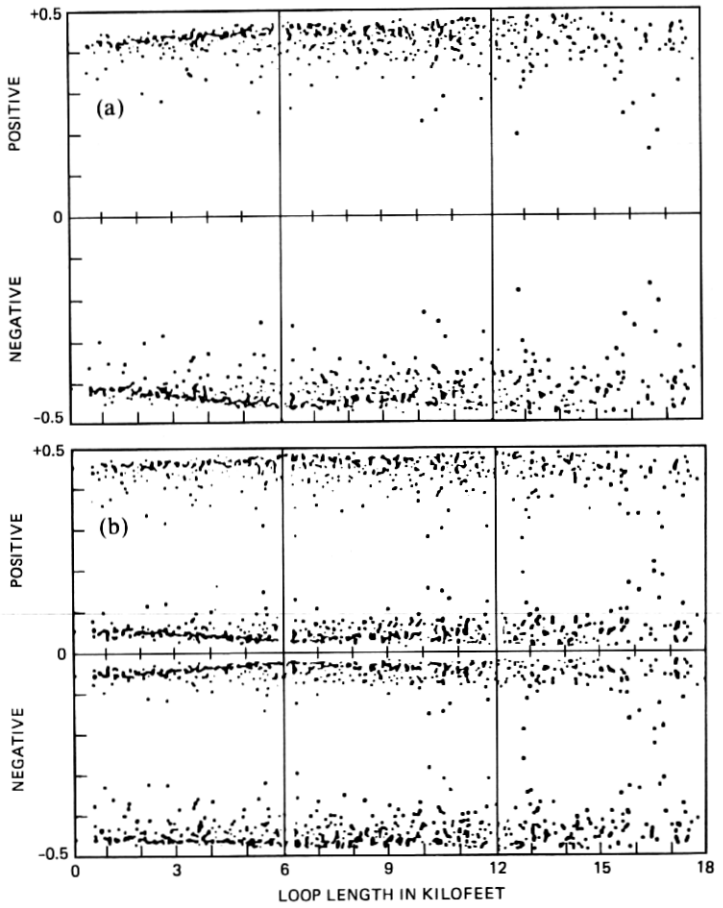

Fig. 27—Eye data scatter plots for 64-kb/s TCM-mode transmission (actual line rate is 144 kb/s). Bridged taps are left intact. Subscriber side data are given. (a) Eye opening. (b) Eye thickness.

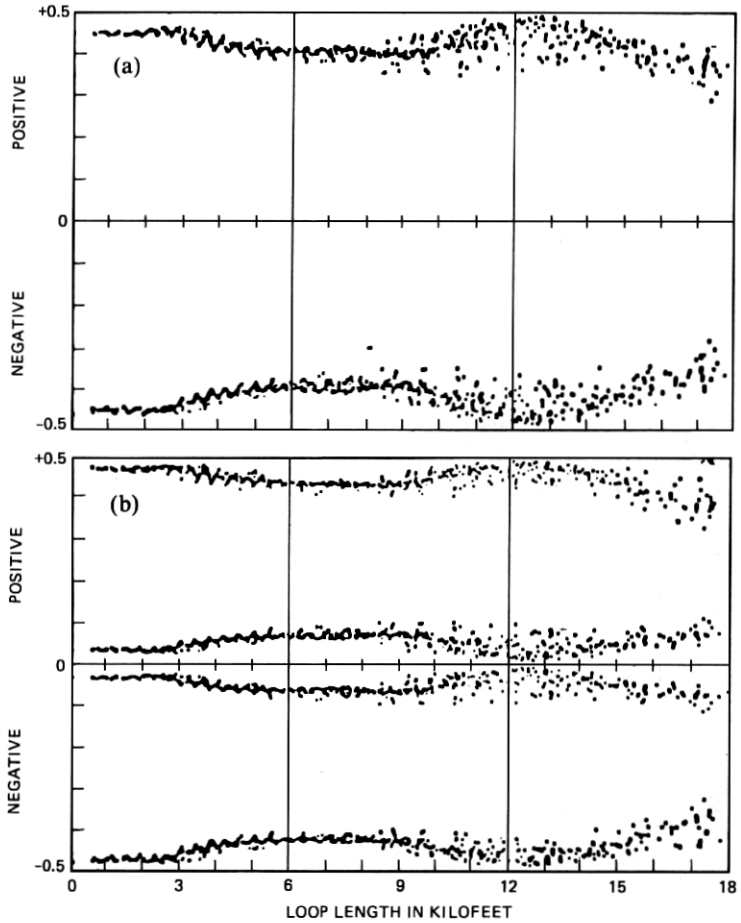

Fig. 28—Eye data scatter plots for 144-kb/s TCM-mode transmission (actual line rate is 324 kb/s). Bridged taps are stripped from the loops. Subscriber side data are given. (a) Eye opening. (b) Eye thickness.

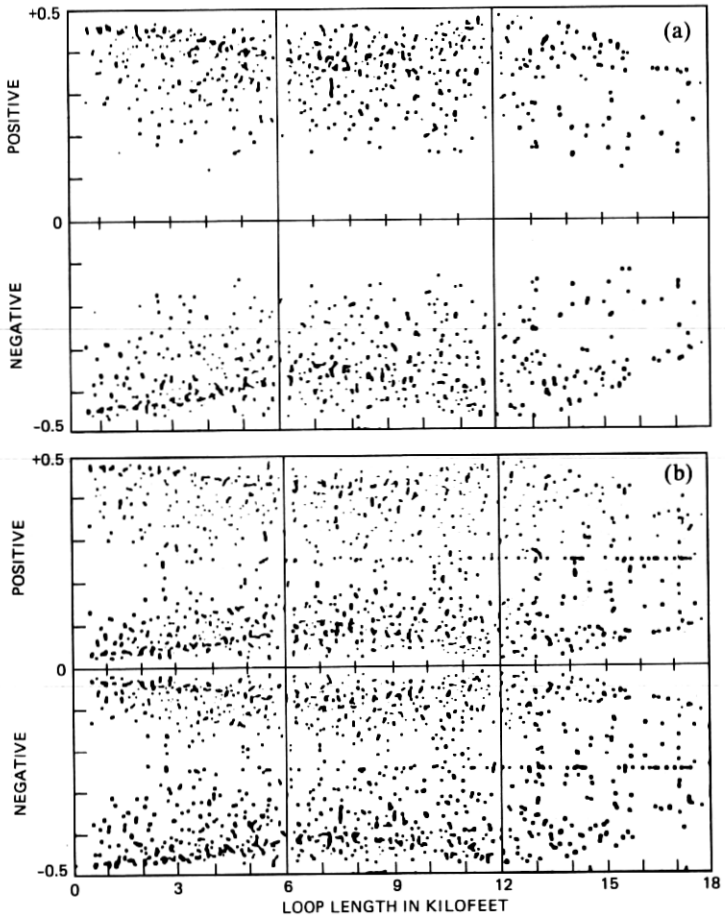

Fig. 29—Eye data scatter plots for 144-kb/s TCM-mode transmission (actual line rate is 324 kb/s). Bridged taps are left intact. Subscriber side data are given. (a) Eye opening. (b) Eye thickness.

VI. ANALYSIS, DESIGN OPTIMIZATION, AND EVALUATION OF EQUALIZERS

6.1 Introduction

Four equalizer designs are analyzed and evaluated for their application to data transmission in the range of 56 to 144 kb/s. The first design is for 144-kb/s transmission. The second design is specifically for a line rate* of 324 kb/s. The remaining two designs are intended for a range of TCM applications in the region of 126 (2.25 × 56) kb/s to 324 (2.25 × 144) kb/s. Realizations of the designs are discussed and

* The information rate is 144 kb/s, but the line rate for this design is enhanced to 324 kb/s because of the TCM operation.

their actual performances are computed by a series of simulation programs discussed in Sections II, III, and IV. To prevent cable mismatch effects (which are indeed present in a hybrid system) from overshadowing the influence of equalization, we present simulation results utilizing continuous unidirectional transmission, thus, focusing on the performance of the equalizer. The equalizers then can be utilized in either a hybrid or a TCM-mode system. The eye-opening scatter plots obtained by analyzing the system performance on actual loops taken from the loop survey are used as the ultimate criteria to judge the equalizer quality.

A digital-system equalizer attempts to undo the effect of cable attenuation and restore the pulse shape at the receiver; however, pulse shape results from a composite of the amplitudes of many frequency components, their phase relationships, and their harmonic relationships. Hence, a perfect pulse restoration at all bit rates entails perfect responses at all frequencies. In essence, an inverse loop circuit constitutes a perfect equalizer circuit. However, loops, bit rates, and coding algorithms are each numerous and uncorrelated, thus, causing additional elements of complexity in the design of equalizers. Even though the results presented here are for the bipolar code, it should be noted that for other codes, the region of spectral emphasis for matching cable loss and equalizer gain will be dictated by the bandwidth requirement of the particular code.

6.2 Three-section, 18,000-ft equalizer

6.2.1 Circuit configuration and representation

Each of the three sections has a five-pole, five-zero circuit. The location of these poles and zeros are obtained by the solution of five simultaneous equations that are formulated to yield exact equalizations of 6,000 ft of No. 22 AWG cable at five discrete frequencies (1, 2, 10, 50, and 100 kHz). Further, the transfer function of the RC circuit is controlled by the gain of an operational amplifier, and this gain is adjusted by yield equalization of loops or loop sections under 6000 ft of cable. Thus, loops of any length under 18,000 ft can be equalized by cascading one, two, or three sections of this equalizer and appropriately adjusting the gains on the three sections of the equalizer. Variation in temperatures is converted to a variation in effective loop length, and the eye height is maintained by the gains of the three sections of the equalizer.

6.2.2 Equalizer performance with composite cables

The performance evaluation of this equalizer with composite cables is limited to a study of eye openings as the composition of the cables is changed gradually for an overall loop length of 18 kft. Two major

simulations are performed. In the first simulation, a loop comprising Nos. 22 and 24 AWG cables with an overall length of 18 kft is chosen. At one extreme, the loop is totally composed of No. 22 AWG cable; conversely, at the other extreme, the loop consists of No. 24 AWG cable. These two cases are presented at the left and right sides of the X-axis in Fig. 30. As the distance along the X-axis is increased, the No. 22 AWG cable is shortened and the length of No. 24 AWG cable is increased. The eye openings are plotted on the Y-axis. The two eyes generated for alternate bipolar coding yield two data points for each loop composition.

Similar results for Nos. 19 and 26 AWG cable compositions are shown in Fig. 31. The simulations are carried out at 144 kb/s. The performance of the equalizer and the quality of the filter are both reflected by the eye opening. The first filter at the transmitting end has the 3-dB point located at half the bit rate. The second identical filter is located at the receiver end. This pair of filters essentially yields a pulse shape, with the amplitude rising from zero and steadily reaching a peak and diminishing to zero, one pulse period after its peak.

In Figs. 30 and 31, a pair of points along each vertical line represents an independent simulation for the appropriate composition of cables. Eye diagrams are internally generated and the seven eye statistics (Section 5.2) are extracted. For each loop, two dots representing the positive and negative eye opening are plotted. From Figs. 30 and 31, it can be expected that the equalizer compensates 18 kft of Nos. 19, 22, 24, and 26 AWG cables with 70, 80, 70, and 0 percent eye openings, respectively. With only No. 26 AWG loops, independent simulations indicate that this equalizer provides an eye opening of about 40 percent with 12 kft loops. It is also interesting to note that the eye openings in either direction of transmission are roughly the same because the effects of reflections (as they occur in a hybrid system) are eliminated, thus, emphasizing only equalizer and filter performances. Proper filter performance is assured by a 100-percent eye opening at zero cable length. The equalizer performance with the loops in the data base may be examined by studying the scatter plots of Figs. 32a and 32b. The eye openings (Fig. 32a) and the eye thickness (Fig. 32b) are generated by the transmission of random data with bipolar codes.

6.3 Four-section, 20,000-ft equalizer

6.3.1 Circuit design

The range and spectrum of equalization are both enhanced for this design. As opposed to the former design, a "staged turn-on" algorithm has been used for more effective equalization. In this mode, the four sections are turned on, one by one, as the range of each section is exhausted by the loop attentuation. Further, the equalization is also

forced out to a frequency of 250 kHz, thus, increasing the total maximum gain from 60 dB for the former design, to about 72 dB. Each section of this six-pole, six-zero equalizer has exact equalization at 1, 2, 10, 50, 100, and 250 kHz for 5000 ft of No. 22 AWG loop.

6.3.2 Equalization data for loop attenuations

The performance of this equalizer is studied at three frequencies. The attenuation of the 831, 1973 survey loops (Section III), in the truncated data base are computed at frequencies of 56, 144, and 324 kHz. Next, the equalization gain for each of the loops at the three corresponding frequencies is also computed. As a next step, the equivalent length of the composite loops, in terms of No. 22 AWG cable, is calculated and the loop attenuations are now plotted in Figs. 33a, 34a, and 35a for these three frequencies at 56, 144, and 324 kHz, respectively. These scatter plots represent approximate straight lines since the gauge-length conversions (see Section 3.4) bring the individual loop attenuation points parallel to the X-axis to roughly fall along the No. 22 AWG cable attenuation line. Finally, the equalizer gains for all the loops are also plotted in Figs. 33b, 34b, and 35b. For perfect equalization, the lines in Figs. 33a and 33b, 34a and 34b, and 35a and 35b should be collinear. The imperfection of equalization is indicated by the noncollinearity of these lines or, for that matter, the nonconcurrence of these individual points.

6.3.3 The 1973 loop survey eye diagram performance

Simulations at 324 kb/s (the TCM mode rate corresponding to 144-kb/s bidirectional hybrid rate) and at 126 kb/s (the TCM mode rate corresponding to 56-kb/s bidirectional hybrid rate) are presented to evaluate the performance of this equalizer. In Fig. 36, the eye openings are shown as a scatter plot of the 1973 survey loops when transmitting data at 324 kb/s in the TCM mode. These results correspond to CO-to-S data transmission. Similar results generated for S-to-CO transmission are not presented. Figure 37 shows the eye-opening data when the system is excited with 126-kb/s TCM mode.

6.4 Limited-range, single-pole equalizer

In the previous two designs the equalizer gain exactly compensates the cable loss at specific frequencies (five for the first, six for the second design) and at specific cable lengths (6 kft of No. 22 AWG and 5 kft of No. 22 AWG cables). Variations because of length are accomplished by changing the gain control on the operational amplifiers. Equalizers reported in Sections 6.4 and 6.5 are designed by broadly matching the shape of the cable loss with frequency against the gain of the equalizer in the frequency domain. Overall gain changed to

accommodate different cable lengths are adjusted by changing diode resistances. This, in turn, adjusts the gain of the operational amplifier without drastically changing the frequency characteristics. A single pole and an adjustable zero-type of transfer function is used to generate a suitable equalization range over a 6- to 36-dB cable loss. When these poles and zero's are redistributed, a corresponding range of equalization may be obtained for these lower frequency applications. The application considered here is for a 324-kb/s TCM-mode data transmission. Cable attenuations and equalizer gains at the half-baud rate (162 kHz) are both plotted in Fig. 38. The dotted lines indicate the cable attenuations of the Nos. 19, 22, 24, and 26 AWG cables. The full lines indicate the corresponding equalizer gain. The chief limiting factor is the range of equalization. The equalizer saturating at about 36 dB cannot compensate for cable losses greater than about 10.7 kft of No. 26 AWG at 162 kHz. Our study of the loop plant indicates that a considerable fraction of loops extends beyond this distance. Hence, the design of this particular type of equalizer has been abandoned for the 324-kb/s TCM mode of bidirectional data transmission. A limited study of eye opening data has indicated that only 30 to 40% of the loops would carry bidirectional data with a 60-percent or better eye opening at 324-kb/s TCM-mode data transmission.

6.5 Enhanced-range, wider-frequency, optimized equalizer

The design philosophy for this equalizer is the same as that for the former equalizer; However, two cascaded, shaped gain amplifiers are used in this case. The first has a low-frequency zero and two higher-frequency poles, while the second has a low-frequency zero, another right-half-plane zero, and a pair of complex poles. However, optimization by the incremental displacement of poles and zeros is essential to follow the loop attenuation at frequencies of interest.

6.5.1 Optimization strategy

An optimization approach in both the frequency and distance domains is simultaneously attempted to match the equalizer gain against the cable loss. First, half-baud rate frequency cable attenuation lines are generated for Nos. 19, 22, 24, and 26 AWG cables. Then the gauge conversion factors (see Section 3.4) at this frequency are used as a basis of all the gauge conversions. The maximum equivalent loop length (as extracted from the loop survey) is then determined to correspond to about 16.7 kft of No. 26 AWG cable. Next, No. 26 AWG cable losses at 5, 10, 50, 100, 150, 200, and 250 kHz are generated by the primary characteristics of the No. 26 AWG cable (see dashed lines in Figs. 39a and 39b). The poles and zeros of the equalizer are given incremental changes such that the equalizer gain and the cable losses

are almost collinear at about the half-baud rate frequency over the span of one-half to two-thirds of maximum cable length (see Figs. 39a and 39b). The first step of optimization is more or less easily achieved; however, in the second step of shifting the R's and C's of the equalizer circuit such that the noncollinearity of the equalizer gain and the cable loss at the low-frequency end of the spectrum has to be weighed against the noncollinearity of the two at the higher end of the spectrum. The optimization becomes complicated by the fact that both the low- and high-frequency noncollinearities themselves display crossovers in the distance domain. Further, the crossover at the low-frequency end has an intersection going from a lower gain to a higher gain as the length of the cable is increased. On the other hand, the crossover at the higher frequency follows an opposite type of characteristic changing from higher gain to lower gain as the distance increases. Thus, a large number of trials are necessary to achieve a satisfactory compromise.

The effect of this optimization implies one distinct effect on the single-pulse response. At lower cable lengths, there is a distinct overshoot because of the higher frequency over equalization and the lower frequency under equalization. Conversely, at longer cable lengths there is a tail left behind in the single-pulse response because of lower frequency over equalization and higher frequency under equalization. But there is a certain range of lengths at which the single-pulse response approaches perfection. We have trapped and exploited this perfection to be about two-thirds the maximum cable length. Thus, the scatter plot generated by this type of equalizer shows nearly 100 percent eye openings (to be discussed next) in the central one-third span of the loops. This type of equalizer behavior is a distinct contrast to those discussed in Sections 6.2 and 6.3. Further, it is consistently good over a range of 126 to 324 kb/s.

6.5.2 Selected loop performance

At 55 ft of No. 24 AWG cable, the eye diagram is imperfect. The cable distortion component can be ruled out at this minimal length. However, in our effort to reduce the circuit complexity, we have eliminated the transmit filter and optimized the pulse width at about 40 percent of the pulse period.* The harmonics of this pulse shape are affected by the receiver filter and by the very slight effect of the equalizer. This has been understood to be the reason for the slight imperfection of the eye diagram shown in Fig. 40 at 324-kb/s operation.

---

* The pulse width for the best eye opening was found to exhibit broad insensitivity in the range of 35 to 42 percent of the pulse period. Hence, for all the simulations, we have held the transmit pulse width at 40 percent and retained a half-baud rate 3 dB down four-section Bessel filter at the receiver end of the loop.

A typical loop response around 6 kft is presented in Fig. 41 at 324 kb/s. In Fig. 41, a seven-section loop with an overall length of 6093 ft is chosen at 60°F. The eye diagram* is relatively the same from both directions of transmission.

Two loops around 12 kft show the response of the equalizer. In Fig. 42, the eye closure is about 18.7 percent at 324 kb/s. This loop is also composed of seven sections and is the worst loop in that region of overall loop lengths. The best system performance also takes place around this length, with a single-section loop with an 11,998-ft No. 26 AWG cable as shown in Fig. 43. The eye closure is only 3 percent, and the response is consistent with the design of the equalizer as discussed in Section 6.5.1.

In Fig. 44, the worst loop (17,314 ft loop) response is shown. The eye closures are about 43 and 42.3 percent for the two sides of transmission, and one can visualize the presence of long tails left behind single pulses in these two eye diagrams.

6.5.3 The 1973 loop survey eye diagram performance

The loops in the truncated loop survey data base have been simulated at four different TCM frequencies (126, 162, 216, and 324 kb/s to correspond to full-duplex bidirectional rates of 56, 72, 96, and 144 kb/s). The scatter plots of eye openings are plotted in Figs. 45, 46, 47, and 48. All these scatter plots exhibit a pattern yielding the best eye openings in the area of the 8 to 13 kft length rather than at about zero length. This particular performance is because of the equalizer optimization strategy.

6.6 Conclusions

The design of the equalizer has a profound effect on the capability of the loops to transmit the digital data. Here, we have compared the various design strategies and studied their effects. An equalizer design using the presently available configurations was optimized for a center frequency of 81 kHz to correspond to 162-kb/s TCM mode. However, a reoptimization of this design at 126 and 324 kb/s was deemed unnecessary because of its satisfactory performance. The optimization procedure described here should prove valuable for the design and implementation of any equalizer configuration, provided its maximum range is adequate for the attentuation expected from the longest of the loops. Effects of cable-bridged taps, impulse noise, and crosstalk on the error rate of the data transmission are not included in this study. If these effects limit the maximum range of equalization, then any of the

* The eye closure is 21.1 percent for the CO-to-S eye diagram and 21.4 percent for the S-to-CO eye diagram.

proposed designs may be effectively used by employing the optimization strategy presented in this paper.

All the simulation results presented here are for the bipolar code. However, it can be visualized that the design philosophy and the optimization techniques are universal to the extent that the region of spectral emphasis (Figs. 39a and 39b) will be dictated by the bandwidth requirements of the particular code.

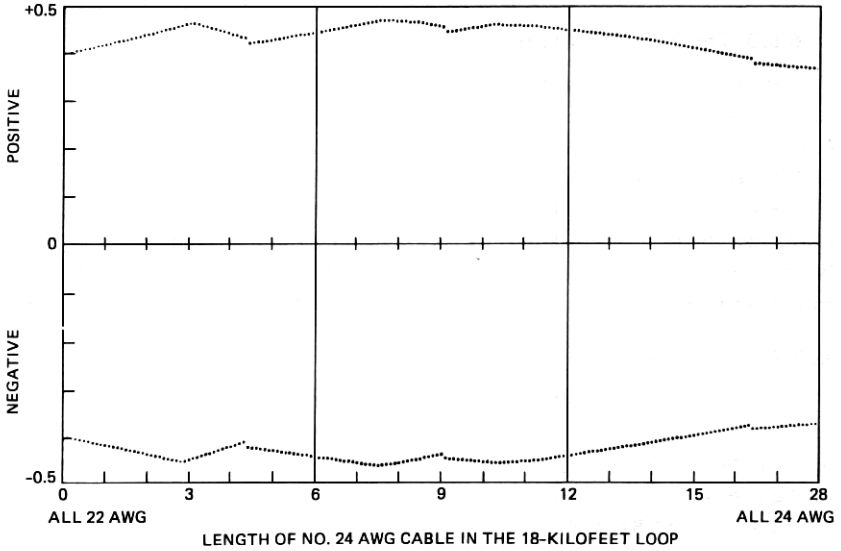

Fig. 30—Eye openings with Nos. 22 and 24 AWG composite cable loops having a total length of 18 kft (144 kb/s).

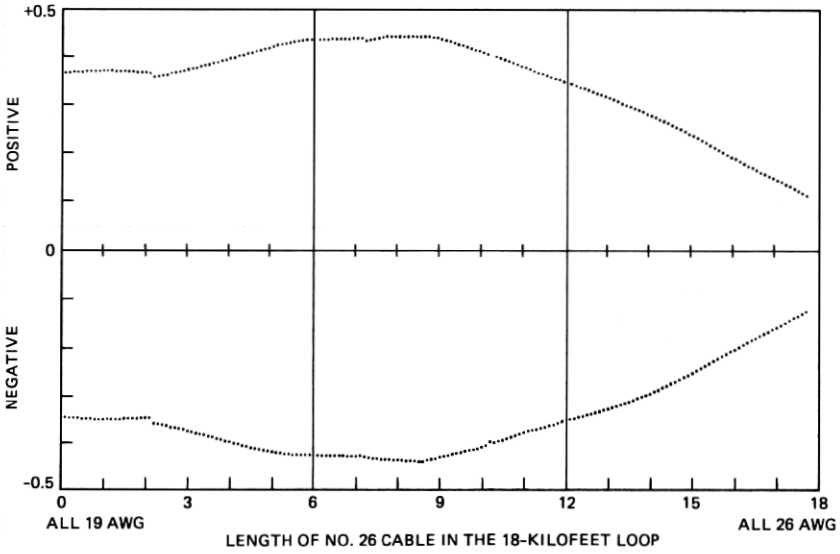

Fig. 31—Eye openings with Nos. 19 and 26 AWG composite cable loops having a total length of 18 kft (144 kb/s).

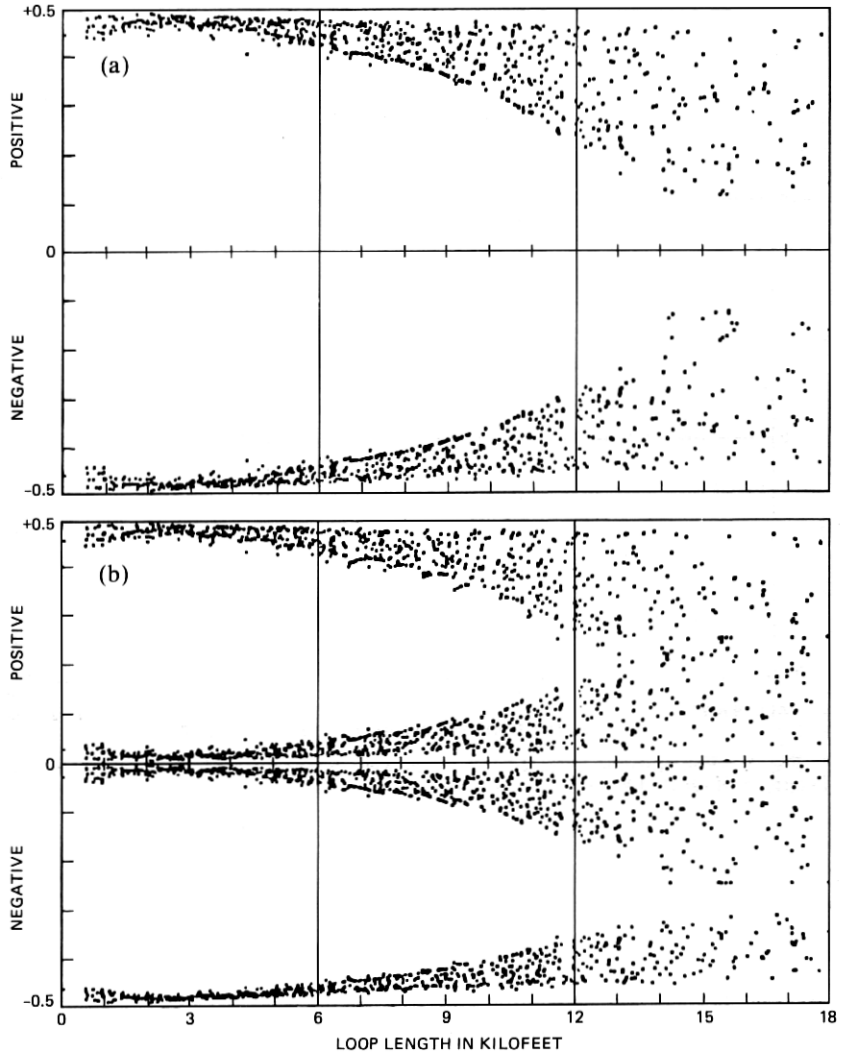

Fig. 32—Eye data scatter plot obtained by the simulation of 1973 survey loops with the three-section, 18,000-ft equalizer at 144 kb/s. (a) Eye opening. (b) Eye thickness.

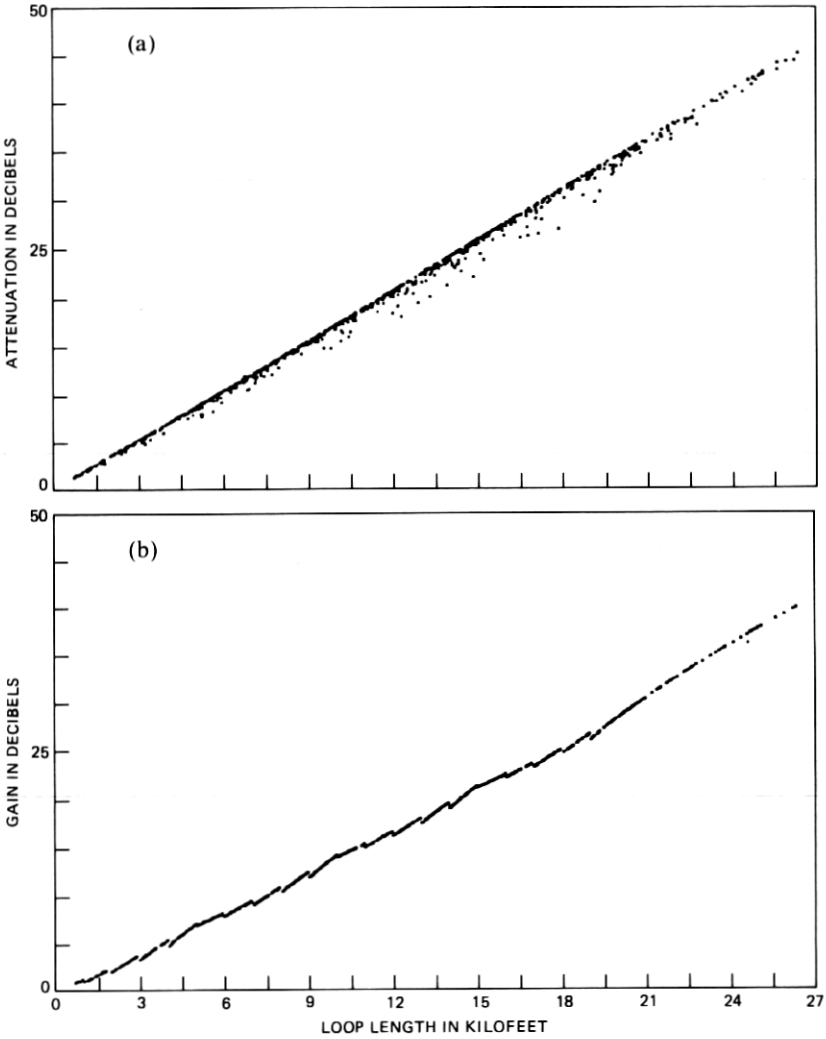

Fig. 33—Comparison of loop attenuations and equalizer gains for 1973 loop survey at 56 kHz plotted against the loop length expressed in equivalent kft of No. 22 AWG cable. Scale on the *Y*-axis is 5 dB/division, and on the *X*-axis it is 1.5 kft/division. (a) Loop attenuation. (b) Equalizer gain.

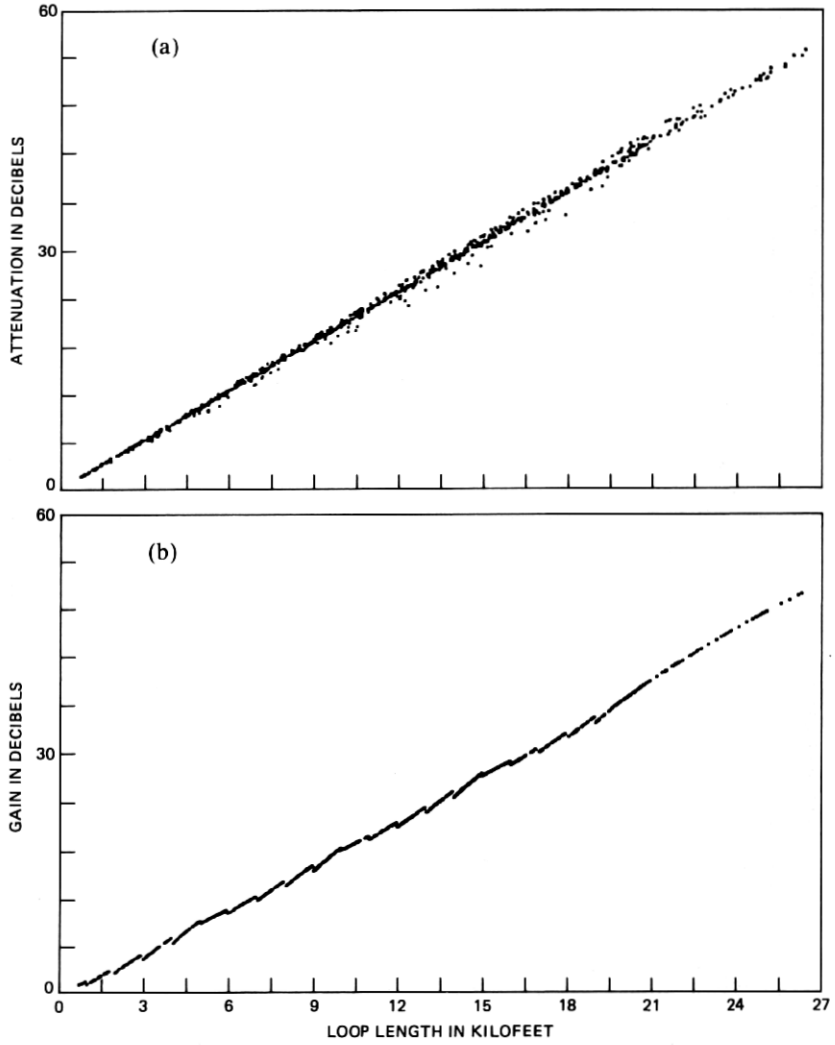

Fig. 34—Comparison of loop attenuations and equalizer gains for various loops at 144 kHz. The *Y*-axis scale is 6 dB/division. (a) Loop attenuation. (b) Equalizer gain.

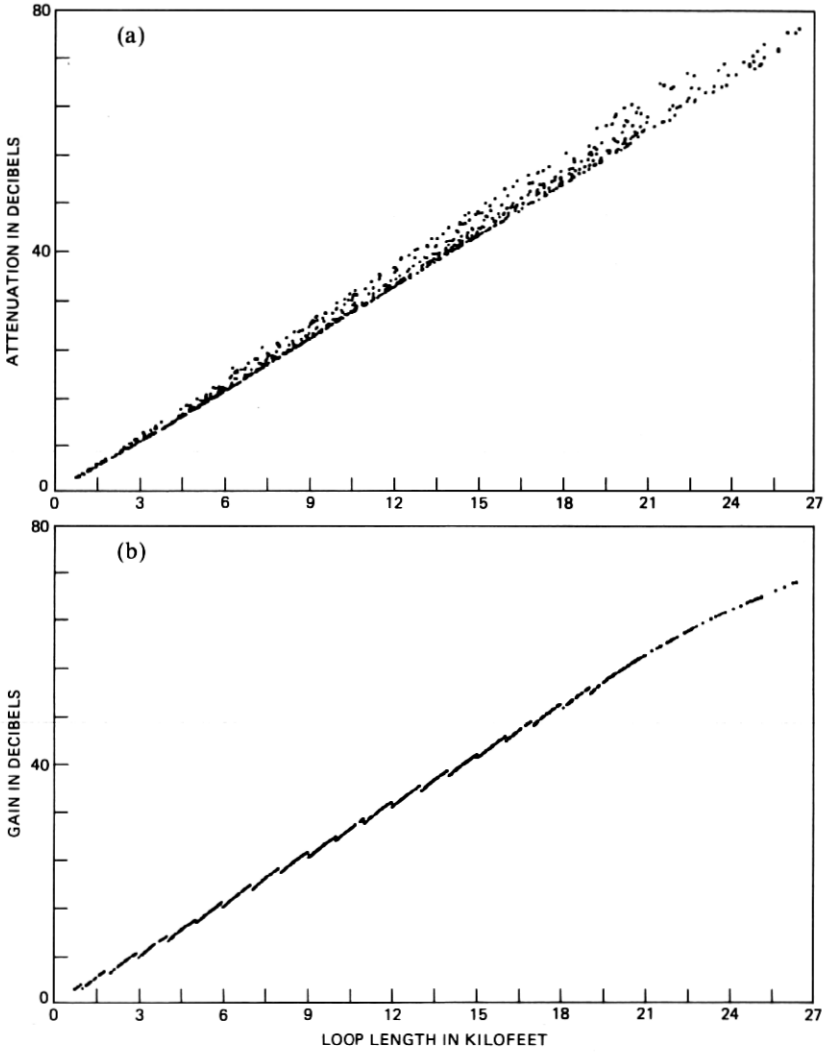

Fig. 35—Comparison of loop attenuations and equalizer gains for various loops at 324 kHz. The *Y*-axis scale is 8 dB/division. (a) Loop attenuation. (b) Equalizer gain.

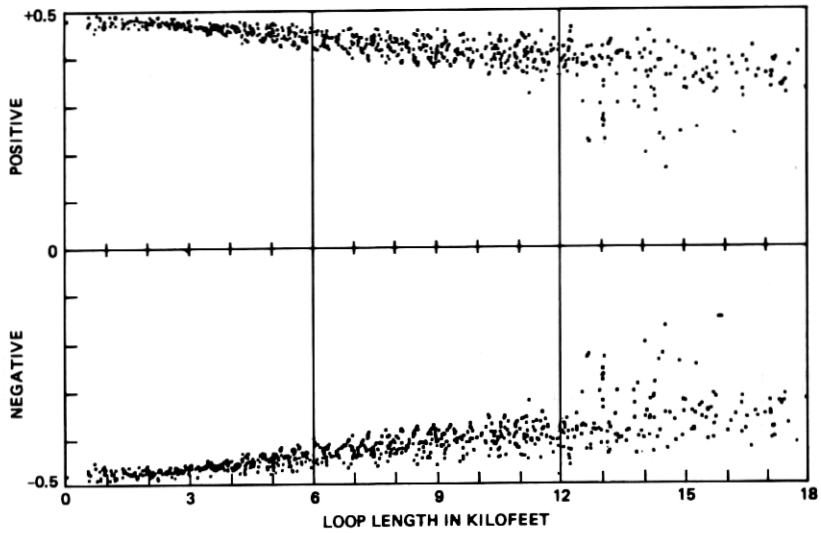

Fig. 36—Eye opening scatter plot at 324 kb/s with 20,000-ft, four-section equalizer in the TCM mode of transmission. Subscriber side data are given.

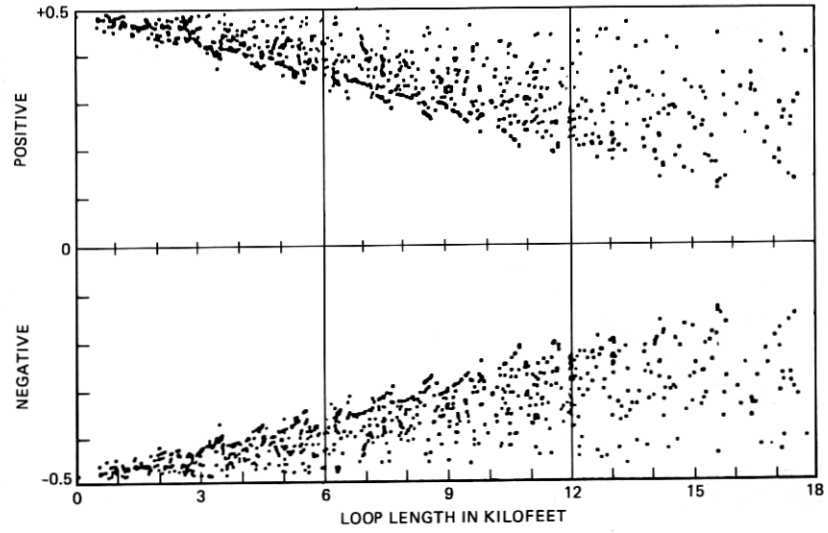

Fig. 37—Eye opening scatter plot at 126 kb/s with 20,000-ft, four-section equalizer in the TCM mode of transmission. Subscriber side data are given.

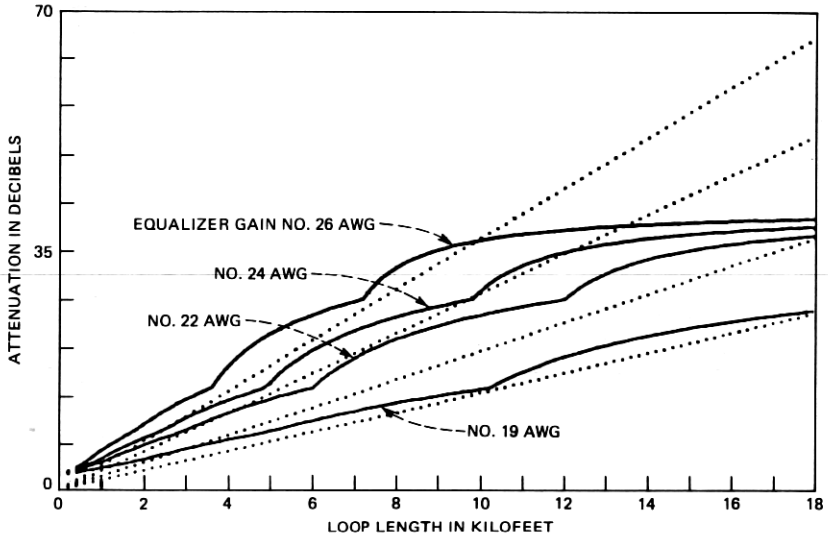

Fig. 38—Cable losses (dotted lines) and equalizer gains of a limited range, single-pole equalizer plotted for a 324-kb/s TCM design. Loop length (1 kft/division) is plotted on the *X*-axis and loop loss (7 dB/division) is plotted on the *Y*-axis.

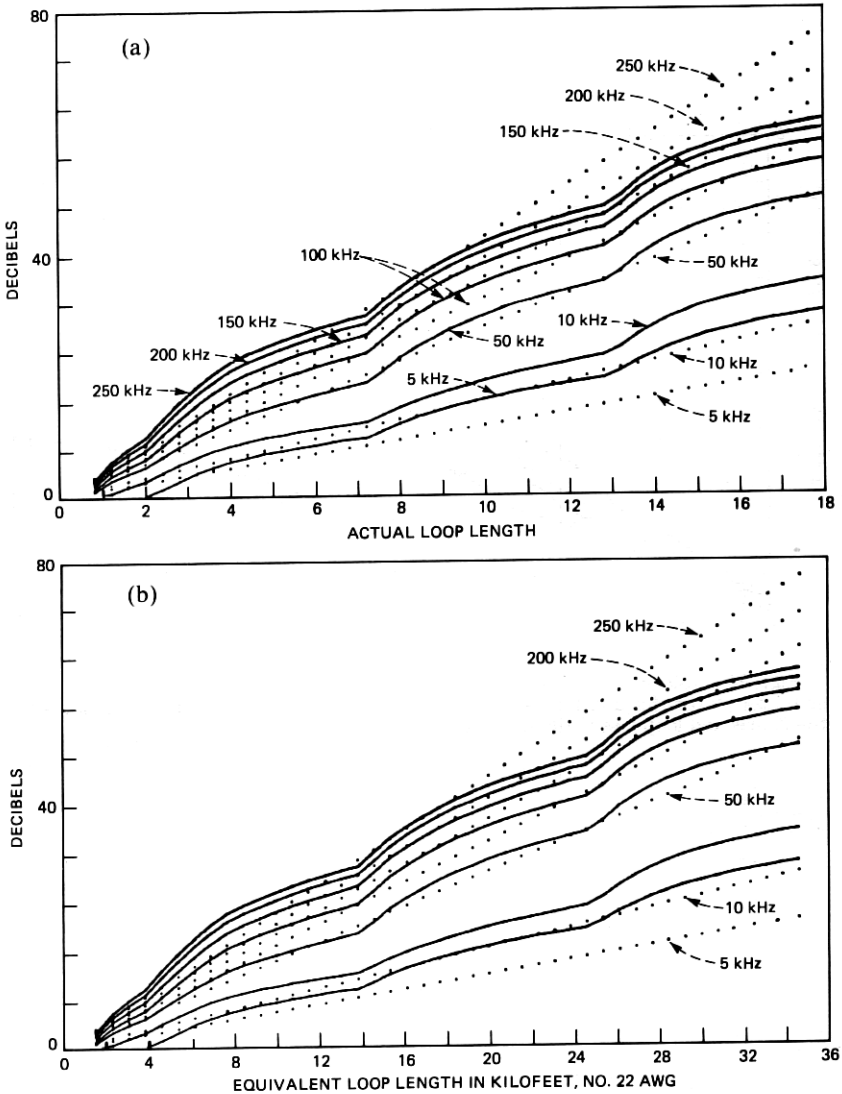

Fig. 39—Comparison of cable loss (dashed lines) and equalizer gains of the enhanced range, wider frequency, optimized equalizer at different frequencies for the No. 26 AWG cable. The *Y*-axis is 8 dB/division. (a) Plot against the actual loop length (the *X*-axis scale is 1 kft/division). (b) Plot against the equivalent loop length in terms of No. 22 AWG cable (the *X*-axis scale is 2 kft/division).

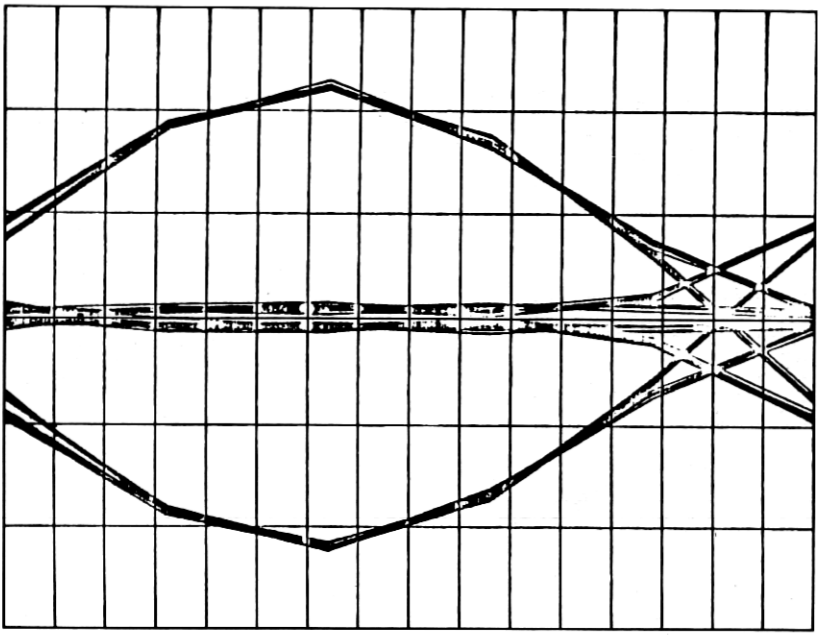

Fig. 40—Eye diagram showing the effect of finite-pulse width with 55 ft of No. 24 AWG cable at 324 kb/s.

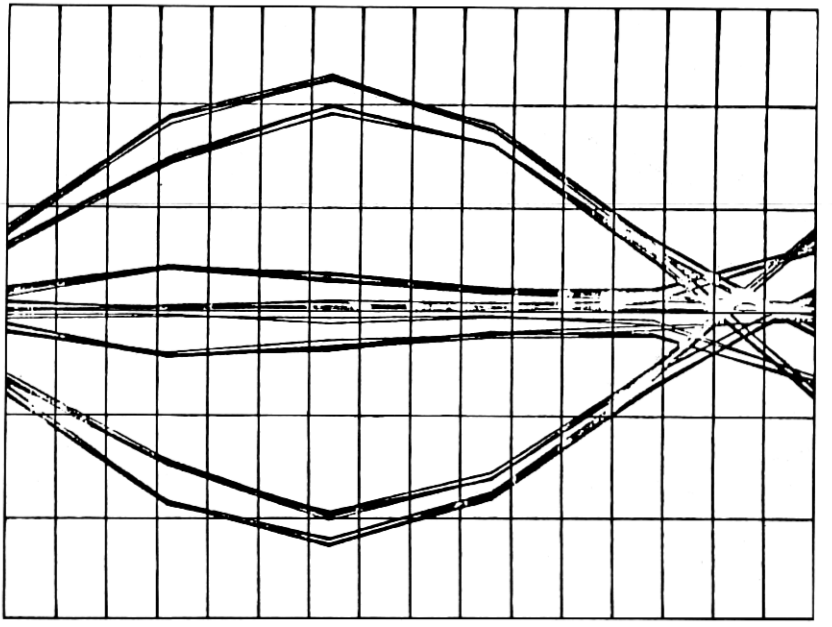

Fig. 41—Seven-section loop (88 ft, No. 19 AWG; 3571 ft, No. 22 AWG; 17 ft, No. 26 AWG; 310 ft, No. 22 AWG; 19 ft, No. 24 AWG, 1299 ft, No. 26 AWG; and 789 ft, No. 24 AWG) response at 324-kb/s TCM excitation.

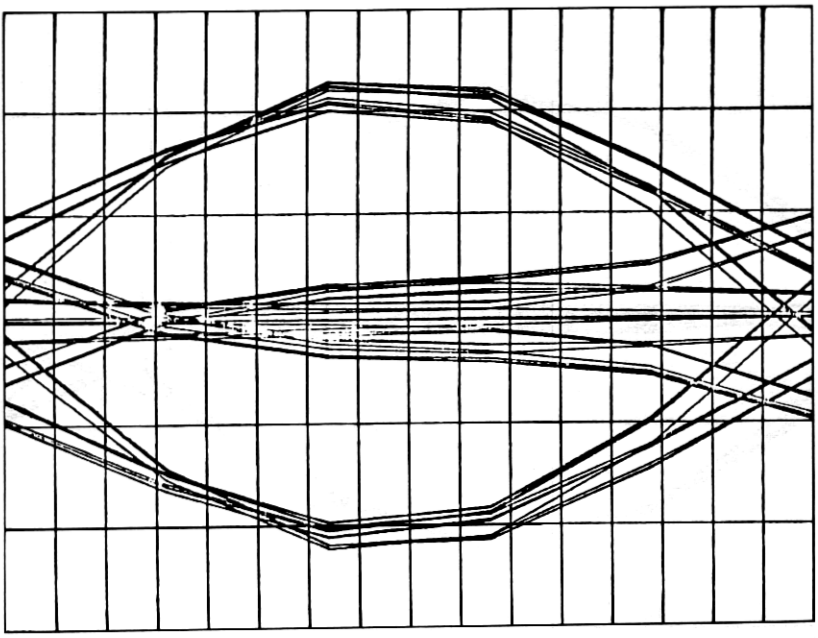

Fig. 42—Seven-section (3450 ft, No. 26 AWG; 261 ft, No. 24 AWG; 50 ft, No. 26 AWG; 313 ft, No. 22 AWG; 2477 ft, No. 24 AWG; 5329 ft, No. 22 AWG; and 200 ft, No. 24 AWG) loop response at 324-kb/s TCM excitation.

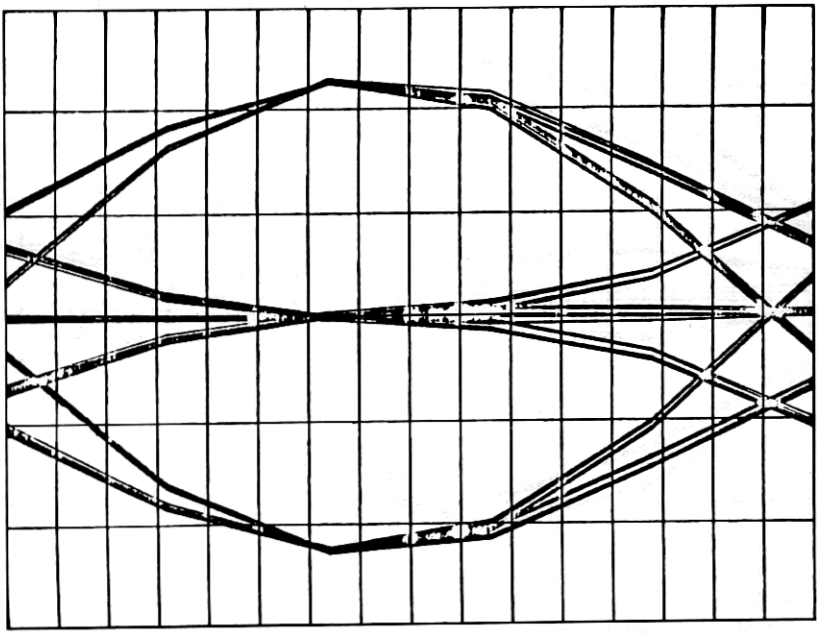

Fig. 43—Eye diagram for a single-section loop consisting of 11,998 ft of No. 26 AWG cable at 324 kb/s.

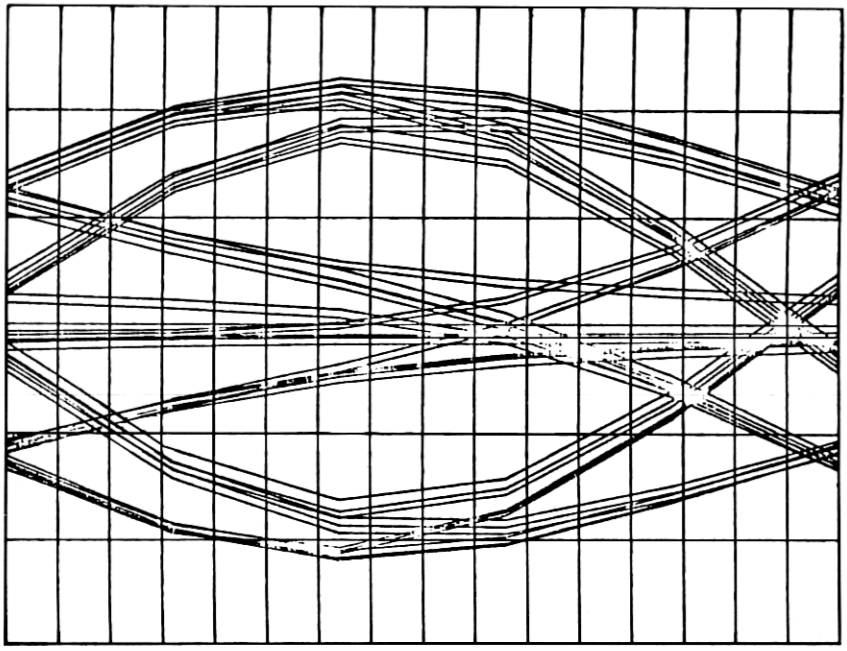

Fig. 44—Worst eye opening for an eight-section (7789 ft, No. 26 AWG; 2998 ft, No. 24 AWG; 2564 ft, No. 26 AWG; 25 ft, No. 24 AWG; 957 ft, No. 26 AWG; 2120 ft, No. 24 AWG; 141 ft, No. 26 AWG; and 720 ft, No. 24 AWG), 17,314 ft loop at 324 kb/s.

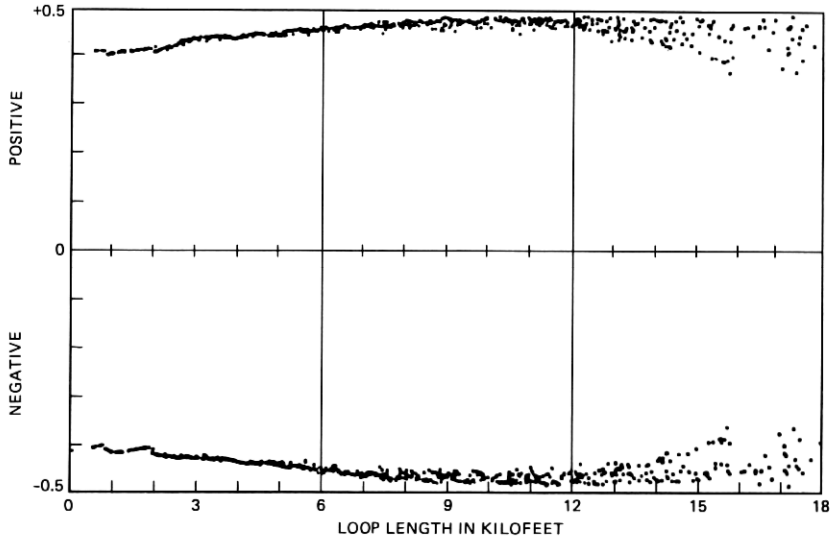

Fig. 45—Eye opening scatter plot for the 1973 survey loops at 126 kb/s TCM mode. (Effective rate is 56 kb/s.)

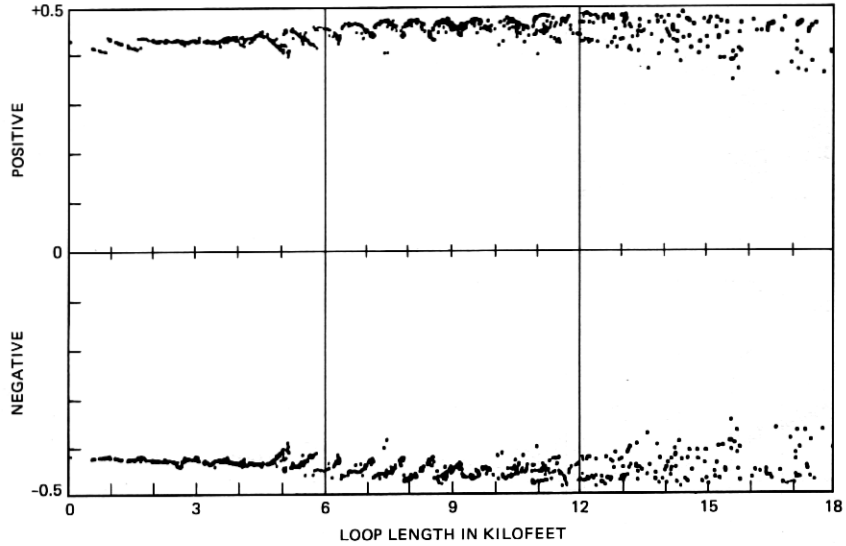

Fig. 46—Eye opening scatter plot for the 1973 survey loops at 162 kb/s TCM mode. (Effective rate is 72 kb/s.)

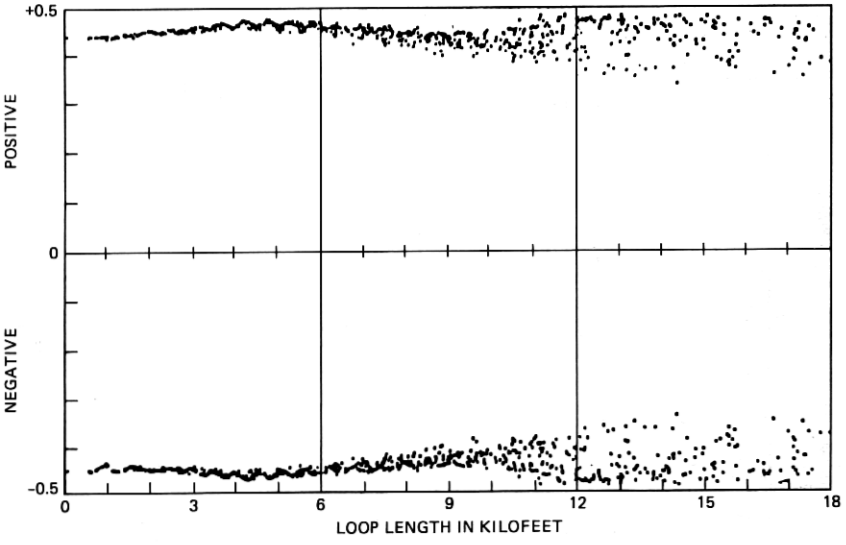

Fig. 47—Eye opening scatter plot for the 1973 survey loops at 216 kb/s TCM mode. (Effective rate is 96 kb/s.)

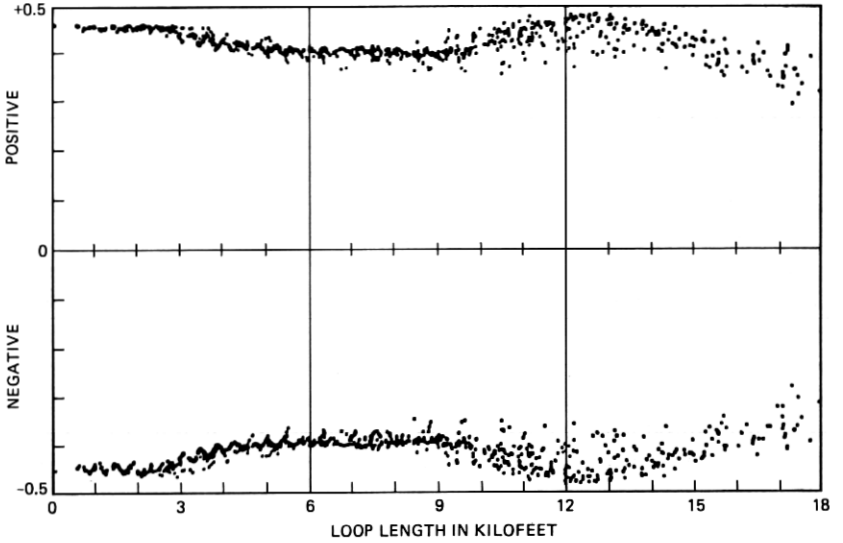

Fig. 48—Eye opening scatter plot for the 1973 survey loops at 324 kb/s. (Effective rate is 144 kb/s.)

VII. CONCLUDING REMARKS

The limit-cycle approach used in the paper and discussed in the Appendixes provides a broad spectrum of results important for the overall design of the digital transmission system. The statistical analysis of the loop plant provides a basis for the design of terminal circuitry, especially for the value of the terminating impedances for a range of transmission rates, and it also indicates the extent of mismatch. For the hybrid system design, this mismatch is the initial basis to choose the quality and extent of echo cancellation. The time-domain response in Section IV is the final basis to study the system performance. The better systems yield a satisfactory eye opening even with the worst configuration of loop studied in Section III. Next, the time-domain simulations over the entire statistically significant population of the loops (Section III) has been cross-compared for the two competing systems (the hybrid and the TCM) at various transmission rates. The summary of these results under two conditions (with bridged taps and without bridged taps) are presented in Section 5.7. Finally, the influence of the equalizer design is clearly indicated in Section VI. It is here that we propose the approach for a systematic design of the equalizer for data transmission. The computer-aided design technique is outlined and the influence of the design strategy is clearly delineated. These designs can be modified and matched with the typical loop environment for the other national telephone networks. Within the

Bell System, the designs have been tailored to the loop environment at data rates between 56 to 324 kb/s.

System design rules vary drastically with the loop environment. Hybrid systems are ideally suited where loop discontinuities are absent. In this case, a low-quality echo canceler can be complimented by an excellent matching circuit. The time-compression mode is suitable for a widely varying loop environment, especially if the extent of the echo cancellation is limited to 30 to 35 dB. Further in the TCM, the extent and persistence of echos at the end of a burst also influences the guard-time duration. Such simulations (even though not reported here) have been conducted[18] and some loops (not essentially those with high-loop losses) have longer time constants for these echos. Acceptable loop configurations in the presence of bridged taps are also critically influenced by the design of the equalizer and filters. For example, the nature of balance that the designer imposes between high-frequency and low-frequency gains (depending on the distribution of the poles and zeros in the equalizer and filters) has a wide ranging influence on the allowable bridged tap(s). Hence, to permit a wide variety of loop acceptance, it is desirable to adjust the equalizer such that the fixed design of the equalizer totally undoes the effect of an average loop with an average configuration of bridged taps. Deviations (because of loop variations) from this perfect compensation causes an error which distributes the eye closure around about a near open eye diagram. It is here that the designer can obtain an acceptable eye opening (about 60 percent) even with the worst loops in the data base by choosing the optimal circuit components. Such designs have also been successfully obtained yielding very low loop failure rates in the TCM mode of transmission.

Further, it is also possible to computationally superpose two independent limit-cycle conditions (one for impulse noise and one for data transmission) to study the effects[18] of impulse noise events on data transmission. The simulations graphically show the influence on the wave shape of the received data and the eye diagram it generates. To study the effects of a typical event on a cross section of the loops in the loop survey data base, we have generated scatter plots of s/n's because of the imperfection of the transmission system with and without the events. High-loss loops suffer more. The nature and harmonic content of the event both influence the error rate. Typically recorded events do not display drastic influence on loops at 64 kb/s (in the TCM mode of transmission) until they reach about a 30-dB loss at 72 kHz. The influence starts to become significant with loops of 40-dB loss—the s/n reduces from 7 to about 3 dB and loops over 40 dB tend to become very unpredictable.

APPENDIX A

Formulations and Component Representation

A.1 Excitation functions

A.1.1 Delta function pulse shape

The mth harmonic of a single-delta function repeating indefinitely, trapped in a limit cycle every T seconds, may be represented as

$$A(p) = a_1 + a_1 e^{-pT} + a_1 e^{-2pT} + a_1 e^{-3pT} + \cdots, \tag{1}$$

where $p = 2\pi \text{im}/T$ and $a_1 = 1$ denotes a positive delta function, $a_1 = 0$ denotes the absence and $a_1 = -1$ denotes the negative-delta function. Further

$$A(p) = \frac{a_1}{1 - e^{-pT}}. \tag{2}$$

The mth harmonic of K such delta-function pulses displaced from the first pulses by τ, 2τ, 3τ, $\cdots$, $k\tau$, $\cdots$, $(K-1)\tau$ seconds can be generalized as

$$B(p) = \sum_{k=1}^{k=K} \frac{a_k e^{-(k-1)p\tau}}{(1 - e^{-pT})}. \tag{3}$$

A.1.2 Finite pulse-width square-wave pulse shape

When a single pulse of width δ repeats infinitely, trapped in a limit cycle repeating every T seconds, then it may be represented as a summation of one positive unit function (repeating infinitely every T seconds) and one negative unit function (also repeating infinitely every T seconds) but displaced by δ seconds. Hence, the algebraic representation of this pulse becomes

$$\begin{aligned} A(p) &= \frac{a_1}{p}[(1 + e^{-pT} + {}^{-2pT} + e^{-3pT} \cdots) \\ &\quad - e^{-p\delta}(1 + e^{-pT} + e^{-2pT} + e^{-3pT} \cdots)] \\ &= \frac{a_1(1 - e^{-p\delta})}{p(1 - e^{-pT})}, \end{aligned} \tag{4}$$

where $p = 2\pi \text{im}/T$ and a_1 (as in Appendix A, section A.1.1) denotes presence or absence of the pulse. For alternate bipolar pulses, the value of a becomes +1, 0 or −1, and for multilevel pulse simulations, a can become q, $(q-1) \cdots 1, 0, -1, \cdots (q-1), -q$, and this would generate a $(2q+1)$ level eye diagram.

The effect of K such pulses $a_1 \cdots a_k$ displaced from the first pulse

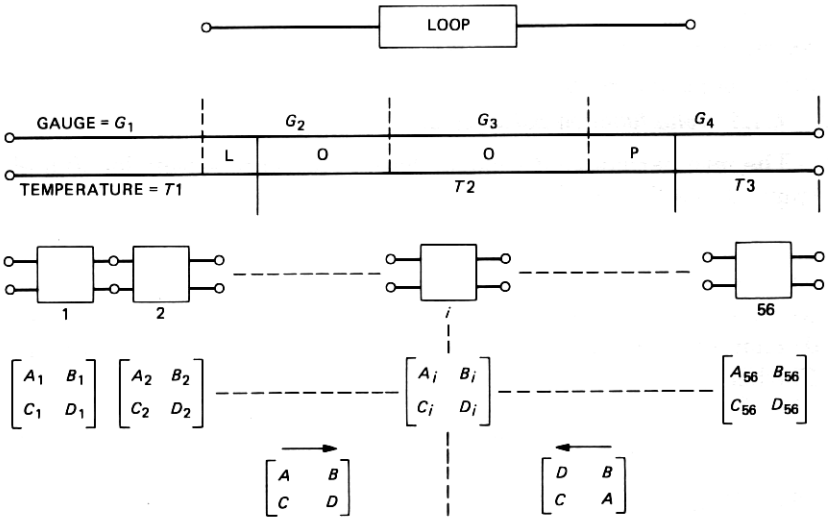

Fig. 49—Loop without bridged taps.

by τ, 2τ, $\cdots$ $k\tau$, $\cdots$ $(K-1)\tau$ can be written as

$$B(p) = \sum_{k=1}^{k=K} \frac{a_k\,(1 - e^{-p\delta})\,e^{-(k-1)p\tau}}{p(1 - e^{-pT})}. \tag{5}$$

APPENDIX B

Loop Calculations

B.1 Loops without bridged taps

In Fig. 49, a loop with four gauges and three temperatures is shown. Fifty-six individual sections are created, each having its own gauge and its own temperature. For these sections, the individual *ABCD* parameters are generated. Composite loop parameters are obtained by matrix multiplication* at each harmonic frequency of the excitation function [See eqs. (3) and (5).]

B.2 Loops with bridged taps

In Fig. 50, a loop with a sections and b bridged taps is shown. Each bridged tap has c sections. This would be the most general representation of any loop without load coils. Only one single temperature is permitted for the entire loop and its bridged taps, to keep the com-

* Each term is complex and should be treated as such.

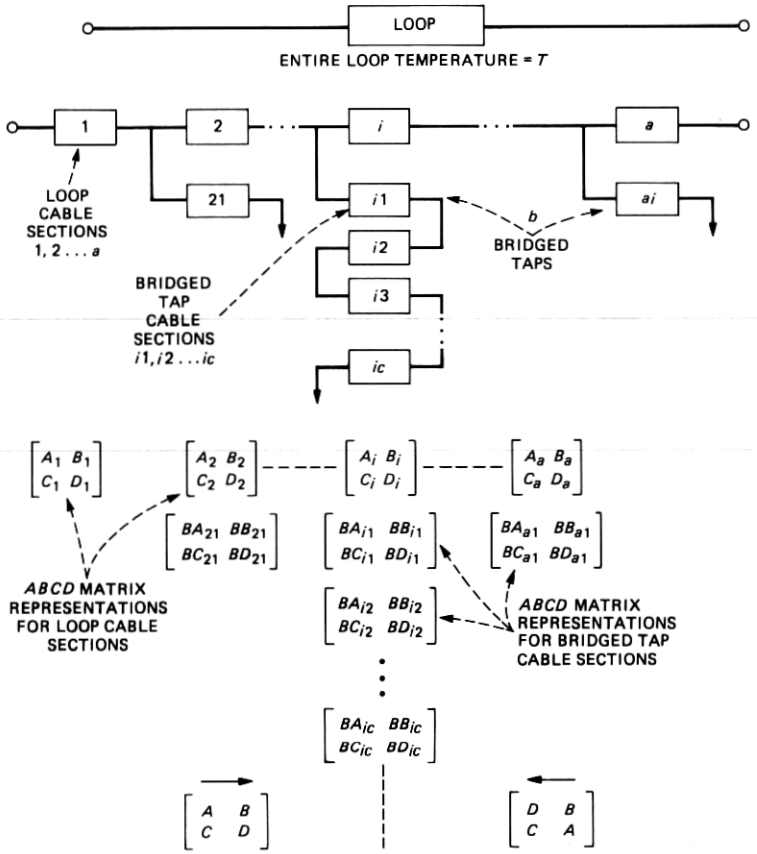

Fig. 50—Loop with bridged taps.

plexity of the representation and to conserve the core space requirements for the computer. Individual *ABCD* parameters for the individual loop section is first generated and stored. When a bridged tap is encountered, its own *ABCD* parameters are obtained by normal *ABCD* matrix multiplication for all the sections in that particular bridged tap. The loop at this point sees the bridged tap as a parallel connection, and the bridged tap *ABCD* is obtained by making A and D unity, B zero, and C as ($Y_0 \tanh \Gamma$), where Y_0 is the admittance (i.e., the square root of CD divided by AB) prior to conversion, and Γ is propagation constant for the entire bridged tap (i.e., the complex log of half the sum of A, D, B/Z_0, and Z_0C, where $Z_0 = 1/Y_0$) prior to conversion.

Thus, the matrix reduction is continued in the presence of the bridged taps, and the net *ABCD* parameters for the entire loop are obtained.

APPENDIX C

Conversion to Time Domain

The system's spectral-domain response can be written as

$$F(p) = B(p) \times \zeta(p), \tag{6}$$

where $\zeta(p)$ represents the system's transfer function for the mth harmonic and p is defined $2\pi\text{im}/T$. The inverse Fourier transform of $F(p)$ is

$$\begin{aligned} f(t) &= \frac{1}{2\pi i}\int_{-i\infty}^{+i\infty} B(p)e^{pt}\zeta(p)dp \\ &= \frac{1}{2\pi i}\int_{-i\infty}^{+i\infty} \sum_{k=1}^{k=K} \frac{a_k e^{-(k-1)p\tau}\zeta(p)e^{pt}dp}{1-e^{-pT}} \\ &= \sum_{k=1}^{k=K}\left[\text{sum of residues at } p = \frac{\pm 2\pi\text{im}}{T}\right]. \end{aligned} \tag{7}$$

For delta functions, we have $B(p)$ defined by eq. (3), and each residue at the mth harmonic can now be evaluated as

$$[a_{-1}]_{m=m} = \lim_{p\to\frac{2\pi\text{im}}{T}}\left(p - \frac{2\pi\text{im}}{T}\right)\sum_{k=1}^{k=K}\frac{a_k e^{-(k-1)p\tau}\zeta(p)e^{pt}}{1-e^{-pT}}. \tag{8}$$

By differentiating the numerator and denominator separately and by L'Hôpital's rule, we have

$$[a_{-1}]_{m=m} = \sum_{k=1}^{k=K}\frac{a_k e^{-(k-1)p\tau}\zeta(p)e^{pt}}{T}, \tag{9}$$

since $e^{-pT} \to 1$ as $p \to 2\pi\text{im}/T$. The summation of residues leads to the time-domain response

$$f(t) = \sum_{m=-M}^{m=+M}\sum_{k=1}^{k=K}\frac{a_k e^{-\frac{(k-1)2\pi\text{im}}{K}}\zeta\left(\frac{2\pi\text{im}}{T}\right)e^{\frac{2\pi\text{im}t}{T}}}{T}. \tag{10}$$

In the earlier computations, M is limited to 64, K is 48. In the more recent computations, M and K have ranged between 64-1200, and 48-480, respectively.

REFERENCES

1. K. Tazaki, K. Okimi, and Y. Hidaka, "COSMOS-1 System—Multiplanning and Local Transmission," Paper presented at Nat. Telecommun. Conf., 1978.
2. N. Inoue, R. Komiya, and Y. Inoue, "Time Shared Two-Wire Digital Transmission for Subscriber Loops," ICC 1979 Conf. Record Paper 2.4, pp. 2.4.1–5.
3. W. Neu, "Long Range Prospects of Digital Subscriber Lines and Sets," Proc. 1978

Int. Zurich Seminar on Digital Commun., IEEE Catalog No. 78 CH-1325-0 ASST, pp. C1.1–5.
4. T. Svenssen, "Methods for Two-Wire Duplex Digital Transmission at 80 kBit/s on Subscriber Lines," Proc. 1978 Int. Zurich Seminar on Digital Commun., IEEE Catalog No. 78 CH-1325-0 ASST, pp. C5.1–4.
5. P. T. Nielson and M. W. Gram, "A Digital Hybrid for Two-Wire Digital Subscriber Loops," Nat. Telecommun. Conf. 1978, IEEE Catalog 1354-0/78/0000–0098, pp. 21.2.1–7.
6. A. H. Ithell and W. G. T. Jones, "A Proposal for the Introduction of Digital Techniques into Local Distribution," Proc. 1978 Int. Zurich Seminar on Digital Commun., IEEE Catalog No. 78 CH-1325-0 ASST, pp. F5.1–5.
7. British Post Office, "Consideration of a Customer's Digital Signaling System," CCITT Study Group XI Delayed Contribution, January 1979.
8. W. A. Kaiser, "Strategies for the Introduction of New Services in Existing Local Networks," Proc. 1978 Int. Zurich Seminar on Digital Commun., IEEE Catalog No. 78 CH-1325-0 ASST, pp. F1.1–10.
9. G. Robin and S. R. Treves, "Progressive Introduction of Digital Switching and Transmission," Proc. 1978 Int. Zurich Seminar on Digital Commun., IEEE Catalog No. 78 CH-1325-0 ASST, pp. F4.1–6.
10. R. K. Even, R. A. McDonald, and H. Seidel, "Digital Transmission Capability of the Loop Plant, ICC 1979 Conf. Record, Paper 2.1, pp. 2.1.1–7.
11. W. E. Danielson and W. B. Macurdy, "Local Digital Switching Trer ds and Design Objectives in the Bell System Network," Conf. Record Int. Switchi g Symp., May 1979.
12. S. V. Ahamed et al., "The Provision of High Speed Digital Data Services Over Existing Loop Plant, " Proc. Nat. Elect. Conf. (November 1979), *33,* pp. 265–70.
13. L. M. Manhire, "Physical and Transmission Characteristics of Customer Loop Plant," B.S.T.J. *57,* No. 1 (January 1978), pp. 35–59.
14. S. V. Ahamed, "The Nature and Use of Limit Cycles in Determining the Behavior of Certain Semideterminate Systems," B.S.T.J. *58,* No. 8 (October 1979), pp. 1869–84.
15. Private communication.
16. E. R. Kretzmer, "Generalization of a Technique for Binary Data Communication," IEEE, Trans. Commun. Tech., *1 CM-14,* No. 1 (February 1966), pp. 67–8.
17. D. J. Clothier and P. Bylanski, "Digital Transmission System for Multiterminal Applications," GEC Telecommun. J., *41* (1980), pp. 10–5.
18. S. V. Ahamed, P. P. Bohn, and N. L. Gottfried, "A Tutorial on Two-Wire Digital Transmission in the Loop Plant," IEEE Special Issue on Communications, *COM 29,* No. 11 (November 1981), pp. 1554–64.